Kinematics of subduction and subduction-induced flow in the upper mantle

W. P. Schellart[1]

Australian Crustal Research Centre, School of Geosciences, Monash University, Melbourne, Australia

[1]   Results of fluid dynamical experiments are presented to model the kinematics of lithospheric subduction in the upper mantle. The experiments model a dense high-viscosity plate (subducting lithosphere) overlying a less dense low-viscosity layer (upper mantle). The overriding lithosphere is not incorporated. Several important features of slab behavior were investigated including the temporal variability of hinge line migration, the kinematic behavior of the slab and the subduction-induced upper mantle flow. Both fixed and free trailing edge boundary conditions of the subducting plate were investigated. Results show that hinge line retreat is a natural consequence of subduction of a negatively buoyant slab. The migration rate increases until the slab approaches the upper-lower mantle discontinuity, resulting in a decrease in migration rate followed by a renewed increase and finally approaching a steady state. Slab retreat results in mantle flow, with material initially located underneath the slab flowing around the lateral slab edges toward the mantle wedge. Experimental results indicate that all rollback-induced flow occurs around the lateral slab edges, forcing the hinge line to attain a convex shape toward the direction of retreat. No signs for poloidal flow underneath the slab tip have been detected. Only a small component of toroidal-type flow was observed underneath slanting slab tips. For a fixed trailing edge, the slab does not sink vertically downward, but sinks at an angle in a regressive manner. For a free trailing edge, slab sinking is oriented more vertically while the surface part of the subducting plate is pulled into the subduction zone.   *INDEX TERMS:* 8120 Tectonophysics: Dynamics of lithosphere and mantle—general; 8122 Tectonophysics: Dynamics, gravity and tectonics; 8121 Tectonophysics: Dynamics, convection currents and mantle plumes; 8150 Tectonophysics: Plate boundary—general (3040); 8155 Tectonophysics: Plate motions—general; *KEYWORDS:* subduction, slab rollback, mantle flow

1. Introduction

[2]   Wadati-Benioff zones and high seismic velocity zones in the Earth's interior indicate that oceanic lithosphere sinks into the mantle, attaining a wide variety of shapes. Focal mechanism data indicate that several slabs continue down to the upper-lower mantle boundary at ~670 km [*Isacks et al.*, 1968]. Tomographic data support this and also reveal that slabs may be horizontally draped over this discontinuity or penetrate even further into the lower mantle [*Spakman et al.*, 1988; *van der Hilst et al.*, 1991; *van der Hilst and Seno*, 1993; *Lucente et al.*, 1999; *Widiyantoro et al.*, 1999; *Wortel and Spakman*, 2000; *Fukao et al.*, 2001].

[3]   Geological and Geophysical data suggest that subducting slabs not only move in a downdip slab-parallel direction (e.g., winglike sliding model [*Jacoby*, 1973]), but

also in a slab-perpendicular backward direction, as has first been suggested by *Elsasser* [1971]. Such a slab-perpendicular backward component would result in regressive (oceanward) hinge line migration of the subducting lithosphere (i.e., slab rollback). Regressive motion could then result in extension in the overriding plate (i.e., backarc extension) due to collapse of the overriding plate toward the retreating hinge line [*Elsasser*, 1971; *Molnar and Atwater*, 1978; *Lonergan and White*, 1997; *Schellart et al.*, 2003]. Thus backarc extension seems to be a direct consequence of slab rollback. It should be emphasized though that when the overriding plate is moving toward the trench and is actively pushes the subducting plate hinge backward (i.e., in the case of the South American plate and the Nazca plate), this results in an increase in seismic coupling between the overriding and subducting plate and induces backarc compression [*Uyeda and Kanamori*, 1979; *Conrad et al.*, 2004].

[4]   As evidenced by the episodic opening of backarc basins [*Faccenna et al.*, 2001a, 2001b] and the wide variety in shapes (from roughly symmetrical to highly asymmetrical) of arc and backarc systems [*Schellart et al.*, 2002a, 2002b, 2002c], it is clear that slab rollback is a transient

---

[1]Now at Research School of Earth Sciences, Australian National University, Canberra, Australia.
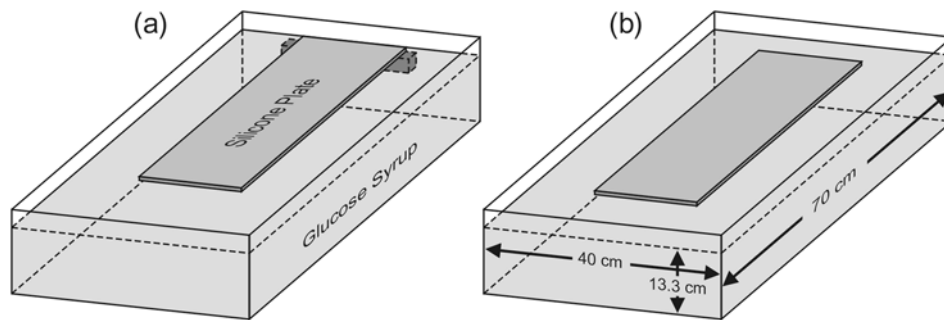
Figure 1. Configuration of the modeling apparatus and experimental setup for two different boundary conditions at the trailing edge of the plate, with (a) fixed trailing edge and (b) free trailing edge. For all experiments, a plate of silicone putty, representing oceanic lithosphere, is resting on top of glucose syrup, representing the sublithospheric upper mantle, down to the bottom of the box, representing the 670 km discontinuity. During an experiment, the first part ($\sim$2 cm) of the tip of the silicone plate is depressed at an angle of $15°-30°$ into the glucose syrup to initiate a subduction instability.

three-dimensional process with significant trench-parallel variations in retreat velocity. This concept is supported by GPS data for several arcs, such as the Tonga arc and New Hebrides arc, indicating a variation in migration rate along the arc [e.g., *Bevis et al.*, 1995; *Taylor et al.*, 1995].

[5] The process of subduction and slab retreat has been investigated with numerical and analogue models previously. In most of the numerical models, slab retreat was externally imposed as a boundary condition [*Garfunkel et al.*, 1986; *Christensen*, 1996; *Houseman and Gubbins*, 1997; *Olbertz et al.*, 1997; *Buiter et al.*, 2001; *Cízková et al.*, 2002] and therefore the self-consistent dynamical behavior could not be investigated. Furthermore, the experiments were two-dimensional, therefore excluding trench-parallel flow around slab edges to accommodate for slab retreat, which is supposed to account for a significant part of slab-induced mantle flow [*Dvorkin et al.*, 1993]. Analogue experiments simulating subduction, however, were executed in three dimensions and the retreat was either imposed [*Guillou-Frottier et al.*, 1995; *Griffiths et al.*, 1995] or allowed to evolve naturally [*Jacoby*, 1973, 1976; *Kincaid and Olson*, 1987; *Becker et al.*, 1999; *Faccenna et al.*, 1996, 1999, 2001b; *Funiciello et al.*, 2002, 2003]. The analogue models were designed to investigate the influence of a stratified mantle on the subduction process [*Guillou-Frottier et al.*, 1995; *Griffiths et al.*, 1995; *Faccenna et al.*, 2001b; *Funiciello et al.*, 2002, 2003], to investigate subducting plate—overriding plate interaction [*Becker et al.*, 1999; *Faccenna et al.*, 1996, 1999], or to investigate hinge migration [*Jacoby*, 1973, 1976; *Faccenna et al.*, 2001b; *Funiciello et al.*, 2002, 2003]. However, none of these investigations has looked in detail at the kinematics of sinking of the slab into the mantle nor have they looked at the kinematics of three-dimensional flow in the mantle that results from such slab sinking.

[6] In this paper, attention is specifically focused on the kinematics of subduction and slab-induced mantle flow. A large number of three-dimensional fluid dynamic experiments were executed and were recorded with digital cameras from three different perspectives (top-view, side-view and bottom-view), in order to obtain a detailed understanding of the three-dimensional evolution of subduction. In the

experiments described in here, subduction and slab rollback were not kinematically imposed but were allowed to evolve naturally and were driven by buoyancy forces only, reflecting natural conditions. These models provide new insights into how the slab sinks into the mantle and into the evolution of the geometry of the slab. The experiments also illustrate in great detail the three-dimensional flow pattern resulting from lithospheric subduction and slab rollback. The advantage of the analogue setup used for the experiments described in this paper is that it is designed to model in three-dimensional space and can therefore account for subduction and slab rollback-induced lateral flow in the mantle in a realistic manner. In addition, the influence of several physical parameters on hinge line migration has been investigated, including slab thickness, slab density compared to the mantle, slab width and trailing edge boundary condition to obtain insight into the optimal conditions for rapid slab rollback.

2. Fluid Dynamic Model

[7] The models are made of a two-layered system with a high-viscosity layer (1.3–2.0 cm thick) overlying a low-viscosity layer (12 cm thick) comprised in a three-dimensional Cartesian model box, as adopted by other analogue modelers [*Kincaid and Olson*, 1987; *Griffiths et al.*, 1995; *Faccenna et al.*, 2001b; *Funiciello et al.*, 2002, 2003]. The model configuration is schematically plotted in Figure 1 and was inspired by models from *Jacoby* [1973], *Kincaid and Olson* [1987] and *Funiciello et al.* [2000]. The upper layer is made of a filled silicon putty (density ρ_{sp} = 1.48–1.56 $\times$ 10^3 kg/m^3), which is a viscoelastic material. With strain rates in the order of $10^{-5}-10^{-3}$ s^{-1}, the material behaves as a nearly Newtonian viscous material (viscosity $\eta_{sp} \approx 2.4 \times 10^4$ Pa·s). The silicone layer simulates a $\sim$65–100 km thick oceanic lithosphere. The viscosity is homogeneous throughout the model lithosphere and therefore represent an average effective value for the entire lithosphere (e.g., thin viscous sheet approach [*Bird and Piper*, 1980; *Vilotte et al.*, 1982; *England and McKenzie*, 1982]). The viscous rheology is an appropriate first order approximation for the lithosphere, since it has been supposed that a

Table 1. List of the Experiments Discussed in the Text and Their Characteristic Physical Properties

Experiment Number	Slab Density ($\times 10^3$ kg/m^3)	Slab Width, cm	Slab Thickness, cm	Trailing Edge	Figure
4	1.480	20	1.3	Fixed	6
5	1.520	20	1.3	Fixed	6
6	1.560	20	1.3	Fixed	6
8	1.520	10	1.3	Fixed	
9	1.520	15	1.3	Fixed	2, 3, 4, 5, 12, 13
10	1.520	20	2.0	Fixed	4, 5, 12, 13
11	1.520	15	1.3	Free	2, 3, 4, 5
12	1.520	20	2.0	Free	4, 5
20	1.505	15	1.3	Fixed	
21	1.535	25	1.3	Fixed	9
22	1.520	5	1.3	Fixed	
23	1.520	25	1.3	Fixed	
24	1.520	15	1.3	Fixed	8
25	1.520	15	1.3	Free	
26	1.520	15	1.3	Free	9

subducting lithosphere acts as a fluid of some sort over geological timescales (millions to tens of millions of years) [*Houseman and Gubbins*, 1997; *Becker et al.*, 1999; *Faccenna et al.*, 2001b].

[8] The lower layer is made of glucose syrup ($\eta_m \approx 1.3 \times 10^2$ Pa·s, $\rho_m = 1.42 \times 10^3$ kg/m^3) simulating some 600 km of low viscosity sublithospheric upper mantle where the base is in accordance with the upper-lower mantle boundary at ~670 km. The lateral edges of the model lithosphere are not attached to the sides of the box to avoid edge effects and to allow for lateral flow around the slab edges during subduction. The base is impenetrable and simulates the upper-lower mantle boundary. This boundary often (temporarily) halts subduction, resulting in horizontal deflection of the slab at the upper-lower mantle transition zone [*Fukao et al.*, 2001] and therefore the simplification seems justified when investigating subduction processes in the upper mantle only. In addition, the upper-lower mantle transition is defined by a factor of 30–100 increase in viscosity [*Davies and Richards*, 1992; *Bunge et al.*, 1996; *Conrad and Lithgow-Bertelloni*, 2002]. Owing to this viscosity increase, slab subduction and subduction-induced flow in the upper mantle will not be influenced much by the applied simplification of the model.

[9] The effects of temperature or phase changes are not considered in the experiments. This approximation has been adopted before [*Becker et al.*, 1999; *Faccenna et al.*, 1996, 1999, 2001b; *Funiciello et al.*, 2002, 2003] and is justified to a first approximation, since the models are restricted to relatively rapid slab subduction in the upper mantle (corresponding to up to ~14 cm/yr), in which the slab retains its thermal field to the first order [*Wortel*, 1982]. Some experimental parameters for the individual experiments discussed in this paper are plotted in Table 1. The difference in viscosity between lithosphere and sublithospheric mantle in the model is a factor of ~185, which is close to values in nature estimated previously (~200 [*Houseman and Gubbins*, 1997], 50–200 [*Conrad and Hager*, 1999], ~100 [*Becker et al.*, 1999], 100–500 [*Faccenna et al.*, 2001a]). The timescale ratio between the analogue model and the natural prototype is $t^a/t^n \approx 3.81 \times 10^{-12}$ (1 hour in model represents ~30 Myr in nature). With such a timescale ratio at hand one can calculate

the upscaled sublithospheric upper mantle viscosity from the following scale relationship:

$$\frac{\eta^a}{\eta^n} = \frac{\sigma^a t^a}{\sigma^n t^n} \qquad (1)$$

where superscript a denotes the analogue model and superscript n denotes the natural prototype, η indicates the viscosity, σ indicates the stresses and t indicates time. Stresses scale as follows:

$$\frac{\sigma^a}{\sigma^n} = \frac{\Delta\rho^a g^a x^a}{\Delta\rho^n g^n x^n} \qquad (2)$$

where $\Delta\rho$ is the density contrast between subducting lithosphere and sublithospheric mantle, g is the acceleration due to gravity and x indicates length. Since the experiments presented in this paper are executed in the Earth's field of gravity, g in equation (2) can be omitted.

[10] Using equations (1) and (2) and the aforementioned timescale ratio t^a/t^n is $\approx 3.81 \times 10^{-12}$, $\Delta\rho^a = 100$ kg/m^3, $\Delta\rho^n \approx 80$ kg/m^3, $x^a/x^n = 2.0 \times 10^{-7}$, and $\eta^a \approx 1.3 \times 10^2$ Pa·s, this results in a sublithospheric upper mantle viscosity in nature of ~1.36×10^{20} Pa·s. This is similar to values of 10^{19}–10^{21} Pa·s suggested for the natural prototype [*Artyushkov*, 1983; *Ranalli*, 1995], indicating that driving forces for subduction (e.g., due to gravity) are properly scaled with respect to the forces resisting subduction (e.g., viscous forces).

[11] Several experiments have been executed with a different lithospheric density (1.48–1.56 $\times 10^3$ kg/m^3, thus $\Delta\rho = 60$–140 kg/m^3) to study the effect of increase in driving force. The density contrast between slab and mantle in nature is thought to be ~80 kg/m^3 for 80 million year old oceanic lithosphere [*Cloos*, 1993]. In addition, the slab thickness has been varied between 1.3 and 2.0 cm (equivalent to 65 and 100 km) to study its effect on subduction kinematics and subduction rate. Also, slab width has been varied for a number of experiments to gain insights into the influence of these parameters on the kinematics of subduction. The slab width was varied between 5 and 25 cm, corresponding to 250 and 1250 km in nature, and can thus be compared with slabs of narrow to intermediate width. The lower range can be compared with slabs subducting underneath the Calabrian and Betic/Rif arcs, which are both ~250 km wide. Examples of wider slabs are the Scotia slab (~600 km), the Hellenic slab (~700 km), the Mariana slab (~1400 km) and the New Hebrides slab (~1500 km).

[12] Passive markers were placed on top and in the side of the silicone layer and on top and inside the glucose layer to track the kinematics of subduction and subduction-induced flow. The experiments were recorded with three digital cameras. The first camera provided a top-view perspective and the second camera provided a side-view perspective. The third camera was installed as such to provide either a bottom-view or a front-view perspective. The camera with the bottom-view perspective of the experiments provided images of fluid motion underneath the subducting plate. With each camera, some 100–150 images were taken during an experiment, which therefore provided a detailed

view of the displacement of the subducting plate and fluid flow in the mantle. At the start of an experiment, the first ~2 cm of the tip of the model lithosphere was manually submerged at an angle of ~15–30° to create a subduction instability. This instability was enough to induce progressive subduction of the lithosphere without any externally imposed force or velocity.

[13] The overriding plate was not modeled to be able to track subduction-induced mantle flow. Thus the influence of the overriding plate on the state of stress at the trench is not incorporated in these experiments. Displacement of the overriding plate toward the trench would induce compression (such as along the South American subduction zone), while displacement away from the trench would induce tension. It should be mentioned, though, that for a large number of subduction settings (Betic-Rif, Calabrian, Carpathian, Hellenic, Kuril, Japan, Ryukyu arc), the overriding plate (Eurasia) has a small absolute velocity (~1 cm/yr [*Jolivet and Faccenna*, 2000]), and therefore the kinematically induced state of stress at the trench is mainly determined by the behavior of the subducting plate. In the experiments, the influence of the subducting plate on the state of stress at the trench can be deduced from the migration of the subduction hinge. Backward (i.e., oceanward) migration of the hinge would induce tensional stresses in the overriding plate and thus would promote extension in the overriding plate (i.e., backarc extension). Forward migration of the hinge would induce compressional stresses in the overriding plate and would therefore promote shortening in the overriding plate. However, the omitting of the overriding plate does imply that the modeled retreat velocity is somewhat high, since the overriding plate is likely to suppress hinge migration.

[14] Two boundary conditions were applied to the trailing edge of the slab, a fixed and a free trailing edge, simulating maximum and minimum resistance of the subducting plate to lateral displacement. The influence of an applied velocity (e.g., ridge push) at the trailing edge of the subducting plate has also been investigated but is discussed elsewhere [*Schellart*, 2003]. The fixed trailing edge scenario can be compared to subduction settings, where the surface part of the subducting plate has a relatively low velocity compared to the hinge retreat velocity of the slab. Examples of the fixed trailing edge scenario in nature are, for example, the Betic-Rif arc [*Lonergan and White*, 1997; *Gutscher et al.*, 2002], the Calabrian arc [*Malinverno and Ryan*, 1986], the Hellenic arc [*Le Pichon*, 1982] and the Carpathian arc [*Royden et al.*, 1983]. In all of these cases, the slab subducting underneath the arc is retreating (or has been retreating in Neogene times) relatively fast, while the velocity of the surface part of the subducting plate is very low. For example, the slabs subducting along the Calabrian arc and Hellenic arc are attached to the African plate, which moves very slow (~1 cm/yr [*Jolivet and Faccenna*, 2000]). In contrast, the rollback rate along the Calabrian arc was ~6 cm/yr for the last 5 Ma [*Faccenna et al.*, 2001b], and the rollback rate along the Hellenic arc is ~3–3.5 cm/yr [*Kahle et al.*, 1998]. Experiments with a free trailing edge are representative of subducting plates with a midoceanic ridge at their trailing edge. Such a

plate boundary offers minimum resistance to lateral displacement of the subducting plate, since the lithospheric thickness at the midoceanic ridge is in the order of only a few km. Some examples of this setting include the Pacific, Nazca, Cocos and Juan the Fuca plate.

3. Results
3.1. Slab Geometry and Kinematics

[15] The evolution of the slab during subduction has been illustrated in Figure 2 and Figure 3 for two reference experiments with different boundary conditions. Both reference experiments have been done three times to ensure reproducibility. Below, the evolution of these experiments will be briefly described.

[16] For experiment 9 with a fixed trailing edge (Figures 2a and 3a), the evolution of the slab geometry is relatively simple. The slab initially sinks and rolls back with an increasing slab-dip angle until it is approximately vertical. When the slab tip hits the bottom of the box, the slab folds backward and is subsequently draped over the horizontal discontinuity during slab rollback. During this stage the slab attains a relatively constant dip angle of ~60–65°. Extensional strain in the horizontal surface part of the plate is observed from displacement of passive white markers in the side and on top of the plate. This extension is oriented perpendicular to the trench and results from the negative buoyancy of the slab (e.g., slab pull). In total, the extensional strain amounts to 6.2% from initiation of subduction until the slab tip approaches the bottom of the box. In addition, the slab part resting on top of the discontinuity is displaced forward, indicating that the slab exerts a push at its frontal part contemporaneously with pulling at the surface part of the plate. During rollback, the slab and trench-line attain a convex arcuate shape toward the direction of slab retreat (Figure 3a), resulting from flow of the glucose syrup around the lateral edges of the slab.

[17] For experiment 11 with a free trailing edge (Figures 2b and 3b), the evolution of the slab geometry is slightly more complicated. The slab initially sinks and rolls back with an increasing slab-dip angle until it is approximately vertical. When the slab tip hits the bottom of the box, the slab tip is slightly overturned, resulting in the formation of a recumbent fold. This is followed by backward folding of the slab and subsequent draping over the horizontal discontinuity during slab rollback. During this stage the slab attains a relatively steep dip angle of ~80°. During subduction, the slab pulls the horizontal surface part of the plate into the subduction zone, as evidenced by the displacement of the trailing edge of the plate toward the trench (e.g., slab pull). No extension is observed in the horizontal surface part of the plate. To the contrary, a slight shortening is observed in the plate, resulting from the buoyancy force between the glucose and the plate. The glucose syrup surrounding the plate has a slightly higher potential energy than the plate itself, and therefore the glucose applies a compression to the plate. About 0.1% shortening strain is observed from initiation of subduction until the slab tip hits the bottom of the box, which corresponds to a time span of ~13 Myr. This results in a shortening strain rate of ~2.4×10^{-18} s^{-1}, which is much smaller than normal geological strain rates of 10^{-16}–10^{-14} s^{-1} and therefore does not seem to be of
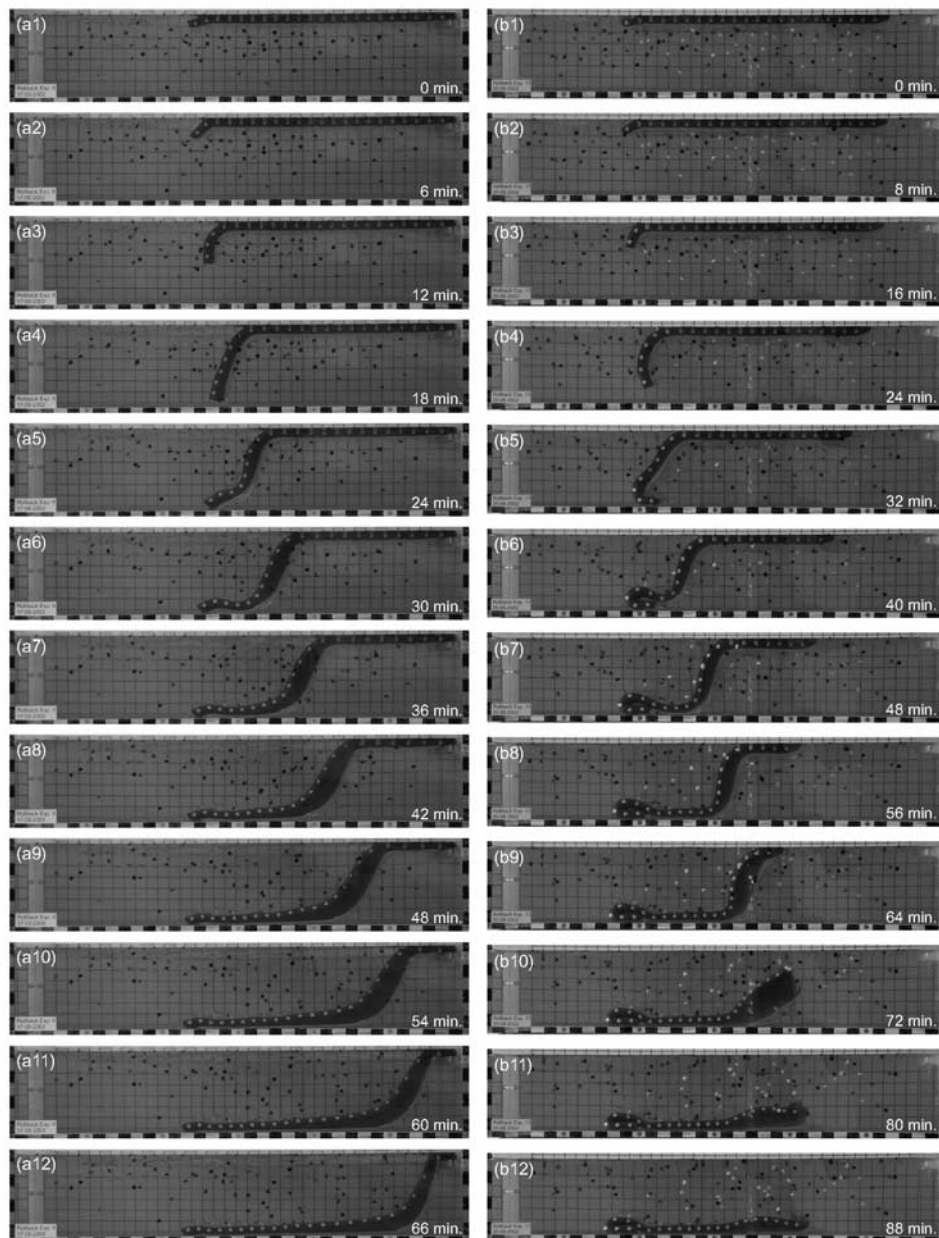
Figure 2. Side-view photographs showing geometrical evolution of the slab during subduction for two experiments with different boundary conditions. (a) Experiment 9 with fixed trailing edge and (b) experiment 11 with free trailing edge. Box is 70 cm long.

geological significance. The slab part resting on top of the discontinuity is displaced forward, indicating that the slab exerts a push at its frontal part. During rollback, the slab and trench line attain a convex arcuate shape toward the direction of retreat (Figure 3b). The arcuate shape is not as well developed as in experiment 9, because the amount of slab retreat is somewhat reduced in experiment 11 compared to experiment 9.

[18] The kinematics of the subduction process for experiment 9 and 11 has been plotted in Figures 4a and 4c. In addition, results from experiment 10 (fixed trailing edge) and 12 (free trailing edge) have been plotted in Figures 4b and 4d, for which the plate is relatively thick (2.0 cm). In these plots, the displacement for passive markers in the side of the

subducting plate has been traced during progressive stages of subduction. All diagrams in Figure 4 show that the subducting slab does not sink in a direction parallel to its own plane but sinks at an inclined angle to its own plane. A difference between experiments with a fixed (experiment 9 and 10) and free trailing edge (experiment 11 and 12) can be observed. The experiments with a fixed trailing edge are dominated by backward sinking vectors (Figures 4a and 4b), while the sinking vectors for the experiments with a free trailing are oriented more vertically, with a smaller component of regressive displacement (Figures 4c and 4d). The difference is most evident for the free sinking stage, before the slab tip hits the lower discontinuity. This sinking behavior can be explained in a purely geometrical way. Initially,
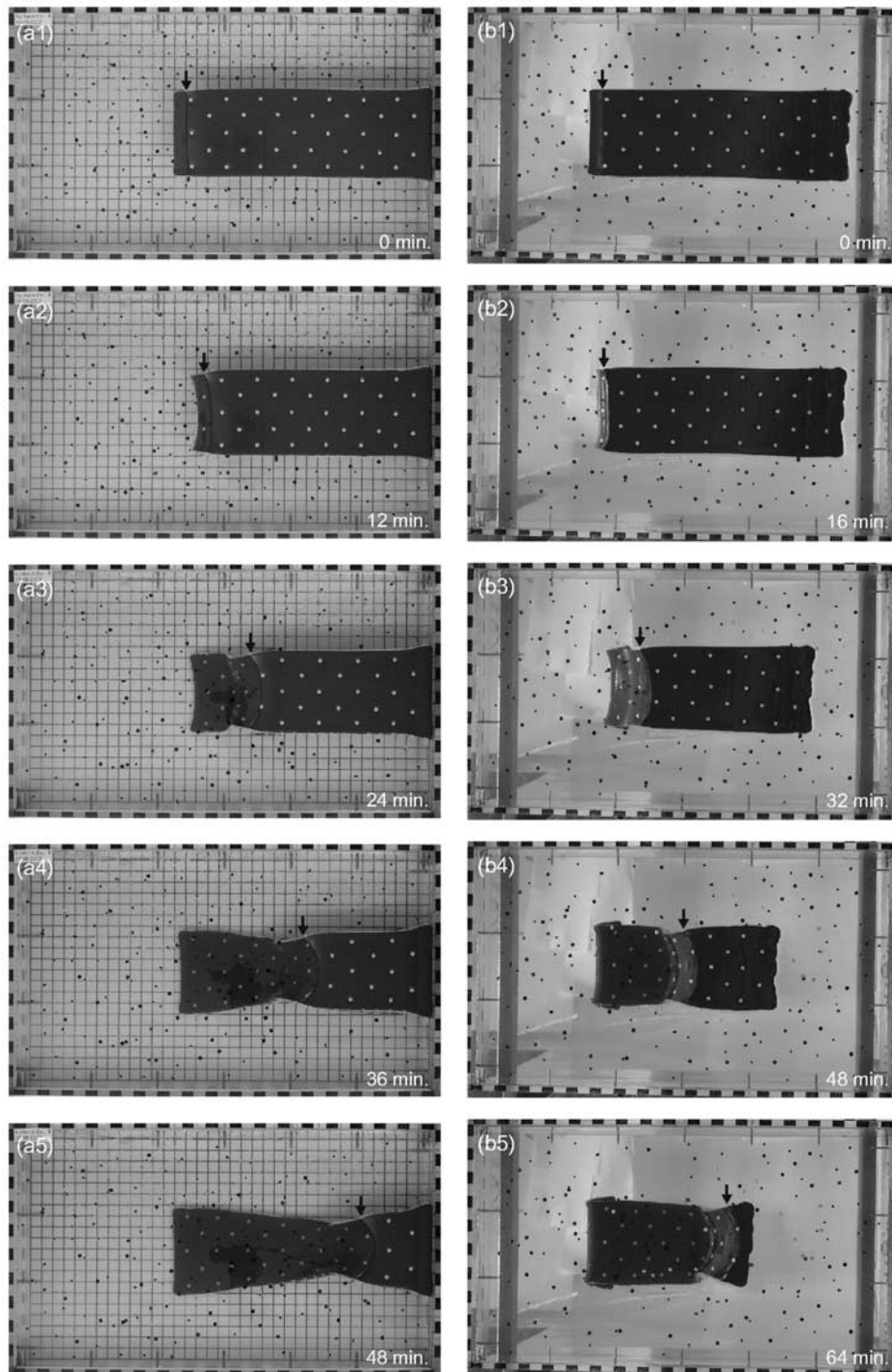
Figure 3. Top-view photographs of two experiments with different trailing edge boundary conditions showing geometrical evolution of the slab during subduction. (a) Experiment 9 with fixed trailing edge and (b) experiment 11 with free trailing edge. Box is 70 cm long and 40 cm wide. Arrows indicate location of trench.

vertical sinking is preferred simply because the gravitational force is oriented vertically downward. However, vertical sinking of the slab requires horizontal displacement of the surface part of the plate. In the fixed trailing edge experiments, the horizontal displacement is resisted significantly, although the plate does experience some extension, resulting

in backward sinking. In the free trailing edge experiments, the horizontal displacement is resisted to a lesser extent (e.g., mantle drag type resistive force) and the surface part of the subducting plate is dragged into the subduction zone, resulting in more vertically oriented sinking. If the mantle drag resistance would be reduced even more (e.g., reduction in
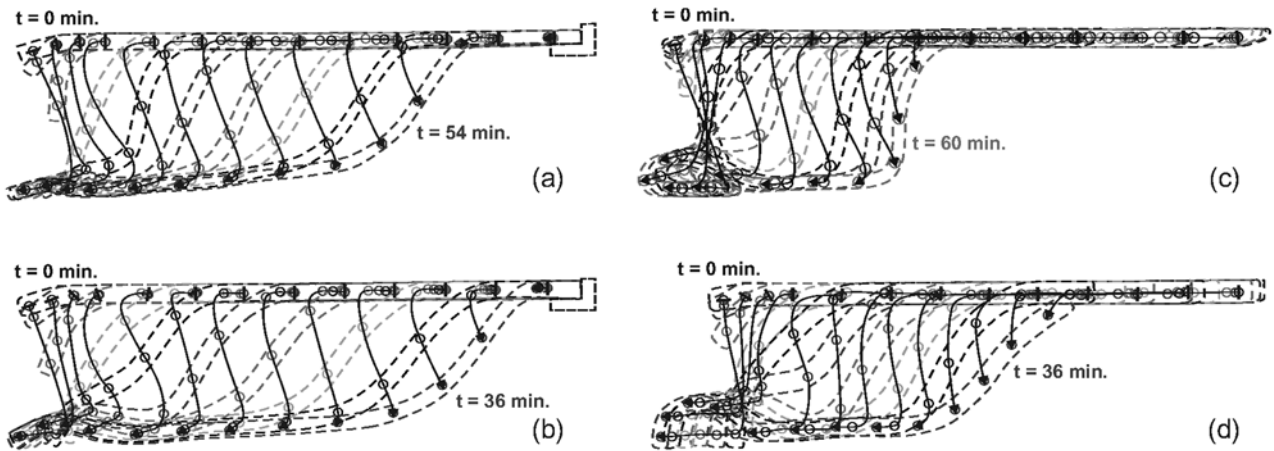
Figure 4. Diagrams illustrating kinematic behavior of the slab and passive particles located on the side of the slab for four experiments with different trailing edge boundary condition and plate thickness. Time step (Δt) between successive stages differs for experiments. (a) Experiment 9 with fixed trailing edge, plate thickness of 1.3 cm and Δt = 6 min. (b) Experiment 10 with fixed trailing edge, plate thickness of 2.0 cm and Δt = 4 min. (c) Experiment 11 with free trailing edge, plate thickness of 1.3 cm and Δt = 6 min. (d) Experiment 12 with free trailing edge, plate thickness of 2.0 cm and Δt = 4 min.

viscosity of the mantle), one would expect the slab to sink vertical or possibly sink forward more parallel to the slab dip.

3.2. Hinge Migration

[19] Hinge migration for experiment 9 and 11 can be observed in Figure 5a. Both experiments show an initial exponential increase in hinge retreat with time, followed by a slowdown in retreat due to interaction of the slab tip with the discontinuity. Subsequently, the retreat velocity increases slightly and finally a steady state retreat is reached with a linear relation between retreat and time. The diagrams illustrate that hinge migration is significantly suppressed for a free trailing edge. For the free trailing edge experiment, the trailing edge displacement curve closely mimics the hinge retreat curve, but the former has a smaller slope angle. The steady state retreat velocity is 46.3 cm/hr and 26.9 cm/hr for experiment 9 and 11 respectively, which scales to ~7.7 cm/yr and 4.5 cm/yr in nature respectively. It
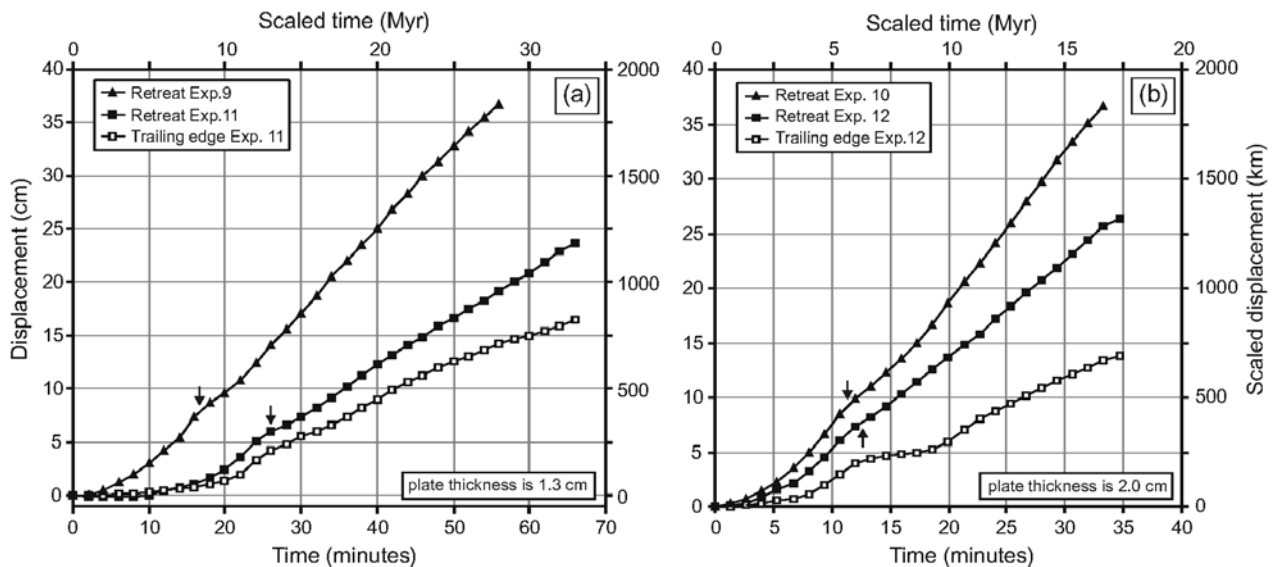

Figure 5. Hinge migration and trailing edge migration versus time for experiments with different plate thickness and trailing edge boundary condition. (a) Experiments with plate thickness of 1.3 cm; experiment 9 with fixed edge and experiment 11 with free edge. (b) Experiments with plate thickness of 2.0 cm; experiment 10 with fixed edge and experiment 12 with free edge. Arrows indicate time when slab tip hits discontinuity. For hinge displacement, positive numbers point to hinge retreat. Note that trailing edge displacement is opposite to direction of hinge retreat, so displacement for trailing edge should actually be read as negative numbers.
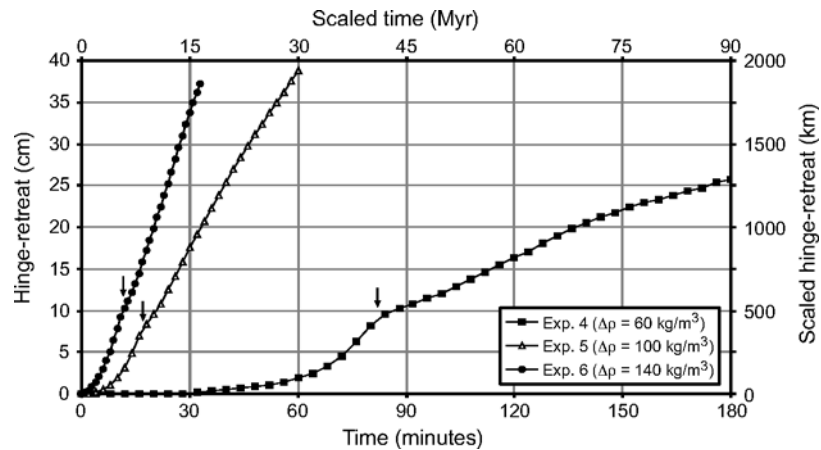
Figure 6. Hinge migration versus time for several experiments with different density contrast ($\Delta\rho$) between slab and surrounding mantle. Arrows indicate time when slab tip hits discontinuity.

should be remembered that these values might be somewhat on the high side, because several factors retarding rollback are not incorporated (e.g., no overriding plate).

[20] The results of experiment 10 and 12 with a relatively thick slab (2.0 cm thick) have been plotted in Figure 5b and show the same behavior as experiment 9 and 11 (1.3 cm thick), but the slabs are retreating at a faster rate. The faster retreat is explained by the greater driving force resulting from the thicker slab. Evidently, the increase in driving force outweighs the increase in strength of the subducting plate due to the increase in plate thickness. The steady state slab retreat increases by a factor of $\sim$1.79 for experiment 10 compared to experiment 9 and $\sim$1.94 for experiment 12 compared to experiment 11, while the thickness increase is in both cases a factor of 1.54. Thus there appears to be no evidence of slowing due to increased bending resistance. In fact, since the retreat factors are in both cases greater than the thickness factor, one could argue that the main resistance to subduction does not stem from the bending resistance. The dominant resistive factor to subduction in these experiments is most likely the resistance exerted by the surrounding glucose syrup [e.g., *Schellart*, 2004]. The faster retreat in experiment 10 and 12 results in a shallower dip during subduction ($\sim$55° and $\sim$60–65° respectively during steady state retreat) compared to experiment 9 and 11 ($\sim$60–65° and $\sim$80° respectively during steady state retreat).

[21] The influence of slab density on the hinge retreat velocity can be observed in Figure 6. From the diagram it is immediately clear that an increase in density contrast between subducting plate and underlying medium increases the hinge migration rate. For the steady state part of the hinge retreat, the average hinge migration velocity (v_{hm}) increases from $v_{hm} \approx 12.6$ cm/hr ($\Delta\rho = 60$ kg/m^3) to $v_{hm} \approx 43.8$ cm/hr ($\Delta\rho = 100$ kg/m^3) to $v_{hm} \approx 81.8$ cm/hr ($\Delta\rho = 140$ kg/m^3). In addition, the hinge migration rate is much more influenced by the interaction of the slab tip with the discontinuity for a low density contrast than for a high density contrast as can be observed from the clear defined kink in the curve for experiment 4 ($\Delta\rho = 60$ kg/m^3) in Figure 6. The slab dip during the steady state hinge retreat was constant and decreased with increasing retreat velocity from $\sim$80° ($v_{hm} \approx 12.6$ cm/hr) to $\sim$70° ($v_{hm} \approx 43.8$ cm/hr) to $\sim$60° ($v_{hm} \approx 81.8$ cm/hr).

[22] The steady state retreat velocity has been plotted against steady state slab dip angle in Figure 7 for a number of experiments (see also Table 2). The diagram suggests that there is a direct correlation between retreat velocity and slab dip angle, even if these different retreat velocities result from different physical parameters and boundary conditions. The data clearly suggest that an increase in retreat velocity is linked to a decrease in slab dip angle. For a slow retreat velocity (10–30 cm/hr) the slab dip angle is $\sim$80–90°, for an intermediate retreat velocity (30–60 cm/hr) the slab dip angle is $\sim$60–80° and for a high retreat velocity (60–90 cm/hr) the slab dip angle is $\sim$50–60°.

[23] An attempt was made to test the influence of the slab width (W) on the hinge retreat rate. The steady state hinge retreat rate was investigated for five experiments with a width of 5 cm (experiment 22), 10 cm (experiment 8), 15 cm (experiment 9), 20 cm (experiment 5) and 25 cm (experiment 23) and all with a constant thickness of 1.3 cm. It was initially expected that the narrowest slab would show the
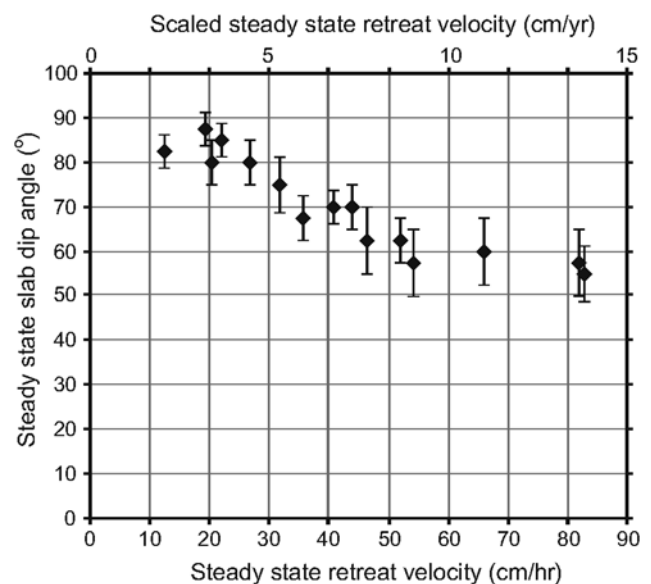

Figure 7. Steady state retreat velocity plotted against steady state slab dip angle for a number of experiments.

Table 2. Experimental Results

Experiment Number	Steady State Retreat Velocity, cm/hr	Scaled Steady State Retreat Velocity, cm/yr	Approximate Steady State Slab Dip	Figure
4	12.6	2.1	80–85°	6
5	43.8	7.3	70°	6
6	81.8	13.6	55–60°	6
8	66.0	11.0	60°	
9	46.3	7.7	60–65°	2, 3, 4, 5, 12, 13
10	82.8	13.8	55°	4, 5, 12, 13
11	26.9	4.5	80°	2, 3, 4, 5
12	52.1	8.7	60–65°	4, 5
20	40.9	6.8	70°	
21	54.1	9.0	55–60°	9
22	19.3	3.2	85–90°	
23	31.9	5.3	75°	
24	35.8	6.0	65–70°	8
25	22.1	3.7	80–90°	
26	20.5	3.4	80°	9

fastest retreat velocity. However, the highest retreat velocity was observed for experiment 8 with a steady state $v_{hm} \approx$ 66.0 cm/hr and W = 10 cm (Table 2). The experiment with the narrowest slab (5 cm) and the experiments with the wider slabs (15, 20 and 25 cm) all retreated slower (Table 2). It should be mentioned that the slab retreat rate and the flow to accommodate slab retreat for the experiment with W = 25 cm (and to a lesser extent also for the experiment with W = 20 cm) was influenced by the lateral boundaries of the model box. For W = 25 cm, the slab edges were only some 7.5 cm separated from the lateral boundaries of the model box. Thus the lateral boundaries might have retarded the rate of slab rollback significantly. Future investigations are required in which experiments have a greater variety in slab width and where the separation between slab edge and lateral box boundary is much greater.

3.3. Subduction-Induced Mantle Flow

[24] Subduction-induced flow was studied in the experiments by tracking passive markers randomly distributed inside and on top of the glucose syrup layer. In particular, the influence of displacement of the slab perpendicular to its own plane (e.g., slab rollback) on mantle flow was investigated. The flow pattern for experiment 24 (fixed trailing edge) can be observed in Figure 8, in which the displacement of a large number of particles (~500) has been traced. The diagrams with the bottom-view perspective show that the flow is dominantly toroidal with two elliptic flow cells illustrating that material initially located underneath the slab flows around the lateral slab edges toward the mantle wedge. Each rotation axis of these cells is located close to one of the lateral slab edges. This type of flow is already observed from the earliest stage of subduction when the slab tip has penetrated down to a depth corresponding to only 100 to 200 km (Figure 8a). The flow pattern does not change in later stages of subduction, when the slab has penetrated deeper into the upper mantle (Figure 8b) or when the slab tip has reached the lower boundary (Figure 8c). The flow velocity does show an increase when Figure 8a is compared with Figures 8b and 8c due to the increase in subduction velocity and rollback velocity in later stages. In the region underneath and immediately in front of the slab,

the displacement vectors are oriented toward the direction of slab rollback. This indicates that rollback-induced flow does not excite any poloidal flow underneath the slab tip toward the mantle wedge to accommodate for the regressive motion of the slab. Rather, slab rollback is entirely accommodated by mantle flow around the lateral slab edges.

[25] From the diagrams in Figure 8 illustrating the side-view perspective, a small component of poloidal flow is observed in the mantle wedge and underneath the slab. This flow results from shearing between the slab and the mantle due to a slab-dip parallel component of displacement. The side-view diagrams in Figure 8 look rather complicated, which stems from the fact that vectors have been plotted for particles located immediately underneath and in front of the subducting plate as well as for particles located at both sides of the subducting plate. In general, particles moving toward the right (i.e., direction of rollback) are located underneath or in front of the subducting plate, while particles moving toward the left are located to the sides of the subducting plate. The side-view diagrams also illustrate that the rollback-induced flow is not strictly toroidal, i.e., the rotation axes of the flow cells are not vertical but are tilted, with the axes oriented subparallel to the lateral edges of the slab. This can be deduced from the additional vertical motion of the passive markers in the side-view diagrams. Right-directed vectors (i.e., the direction of rollback) located underneath and closely in front of the slab generally have an additional significant downward component of motion, while left-directed particles generally have an additional upward component of motion. These upward and downward directed components of displacement result from the rollback process and are not related to the displacement of the slab parallel to its own plane.

[26] The diagrams in Figure 8c illustrate the side-view and bottom-view flow pattern just after the slab tip has hit the bottom of the box. Except for the magnitude of displacement vectors, the flow pattern in Figure 8c is very similar to the flow pattern in Figures 8a and 8b. The similarity in flow pattern confirms the initial observations that all slab rollback-induced flow occurs around the lateral edges of the slab and that no flow occurs underneath the slab tip. This is further supported by the orientation and geometry of the slab near the tip, which was close to vertical and either straight (Figures 2a, 4a, 4b, 4d, 8, and 9b) or concave (Figures 2b, 4c, and 9a) toward the direction of slab retreat in all experiments. If significant slab rollback-induced flow underneath the slab tip would have occurred, the slab tip would have been convex toward the direction of retreat, as was observed for the lateral edges of the slab along which flow did occur (Figure 3).

[27] The flow pattern for experiment 26 (free trailing edge) can be observed in Figure 9a. The flow pattern appears more complex than in the fixed trailing edge experiments due to the large component of slab-dip parallel displacement of the subducting plate. This results in a better defined poloidal component of flow with two flow cells divided by the slab in the middle. One cell is located in the mantle wedge area and the other is located underneath the subducting plate. Two toroidal flow cells are also observed akin to what was observed in experiment 24 with flow around the edges of the slab to accommodate for slab rollback. Again, no rollback-induced flow underneath the
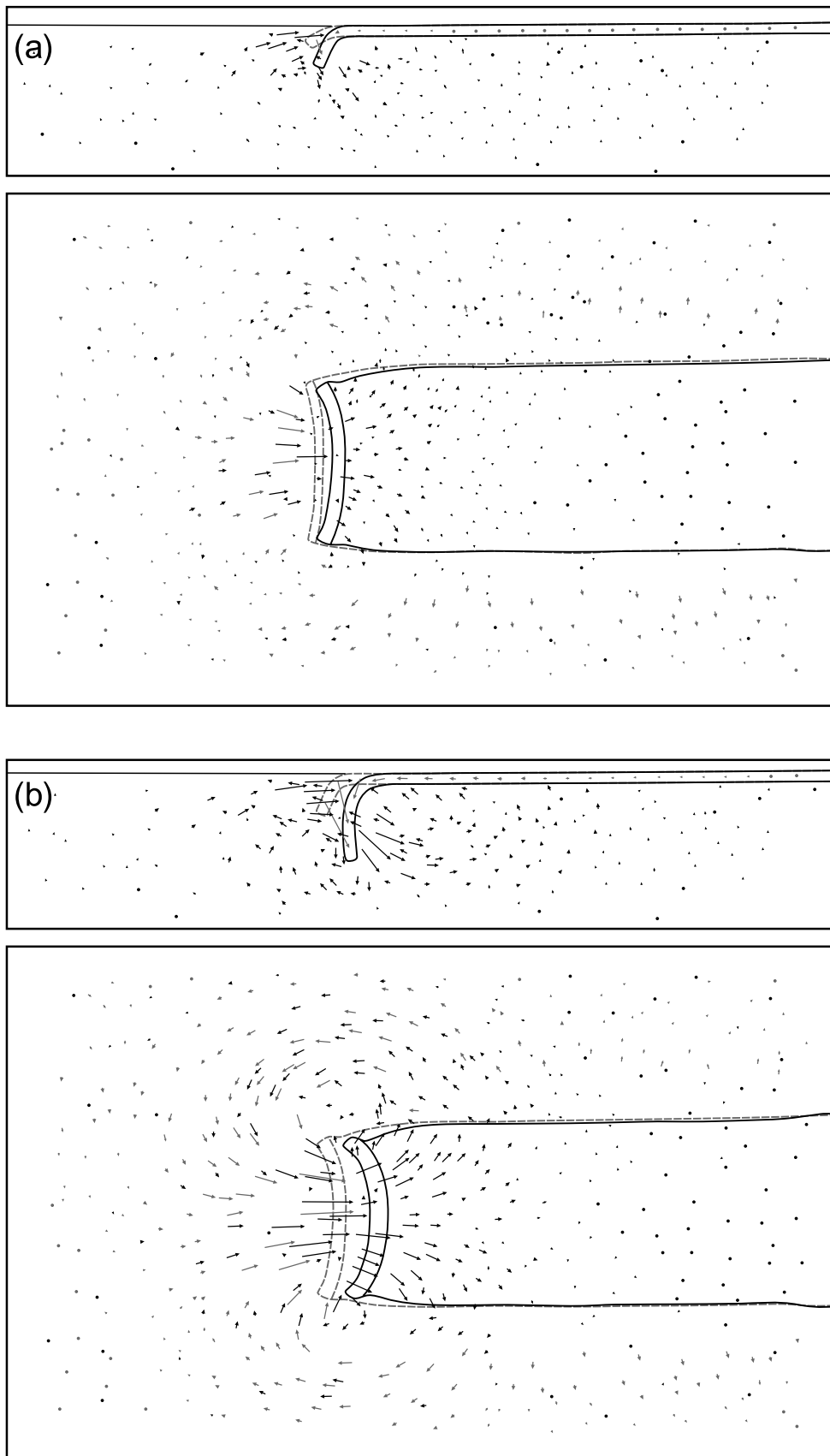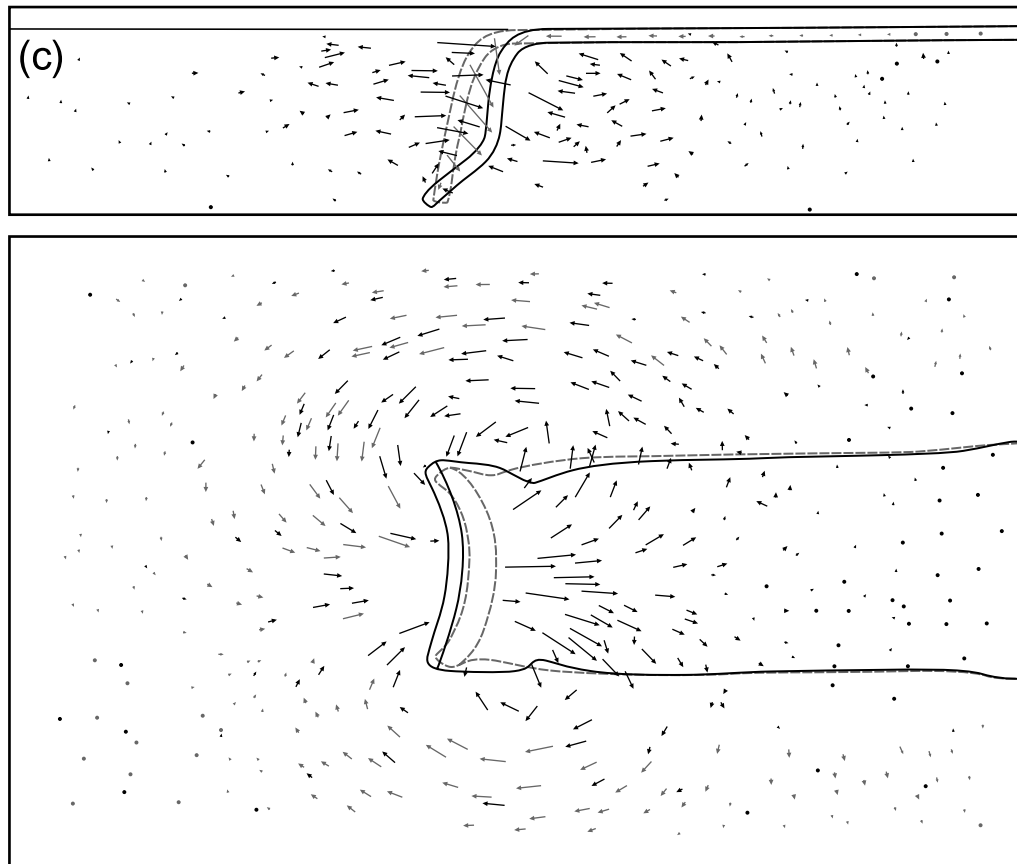
Figure 8

Figure 8. Line drawings of side-view and bottom-view perspective of experiment 24 (fixed trailing edge), illustrating subduction-induced flow pattern in glucose syrup during three stages of subduction. (a) Early stage of subduction between t = 4 min and t = 10 min with subduction depths corresponding to ∼100 and ∼200 km respectively. (b) Intermediate stage of subduction between t = 10 min and t = 16 min with subduction depths corresponding to ∼200 and ∼375 km respectively. (c) Late stage of subduction between t = 20 min and t = 26 min after slab tip has hit the lower boundary corresponding to ∼670 km depth. Vectors indicate amount and direction of displacement of passive markers. Dots indicate no displacement of passive markers. Black vectors are for passive markers in the glucose syrup while gray vectors are for passive markers floating on top of the glucose syrup (bottom view) or passive markers in the side of subducting plate (side view). Shaded dashed lines and continuous black lines illustrate subducting plate contours at the beginning and end of the time lapse, respectively. Please note that in the side-view diagrams vectors have been plotted for particles located immediately underneath and in front of the subducting plate as well as for particles located at both sides of the subducting plate. In general, particles moving toward the right (i.e., direction of rollback) are located underneath or in front of the subducting plate, while particles moving toward the left are located to the sides of the subducting plate.

slab tip is observed during the entire duration of the experiment.

[28] Only in two experiments (21 and 23), a small component of toroidal-type flow underneath the slab tip was observed. This has been plotted in Figure 9b, which shows the flow pattern of experiment 21 in a stage well before the slab tip has hit the bottom of the box. The overall flow pattern is very similar to experiment 24 (Figure 8). However, near the slab tip close to one edge of the slab, the displacement vector of one particle (encircled) is oriented slightly toward the tip line pointing to flow underneath the slab tip. It should be noted that for this experiment (as well as experiment 23), the penetration depth of the slab tip was not constant along the trench (e.g., slanting slab tip line) and

the difference in penetration depth amounted up to 3−4 cm from the northernmost part of the tip line toward the southernmost part of the tip line. The small component of toroidal flow underneath the slab tip was observed underneath the shallowest part of these slanting slab tips. The amount of flow underneath the slanting slab tip was estimated from the magnitude and orientation of the vectors on the side of the slab edges and from the magnitude and obliquity with respect to the slab tip line of the encircled vector in Figure 9b. With a difference in penetration depth of ∼3 cm for the slanting slab tip, it was estimated that flow underneath the slanting slab tip accommodated only ∼5% of rollback-induced flow, while the remaining ∼95% of the flow occurred around the lateral edges of the slab.
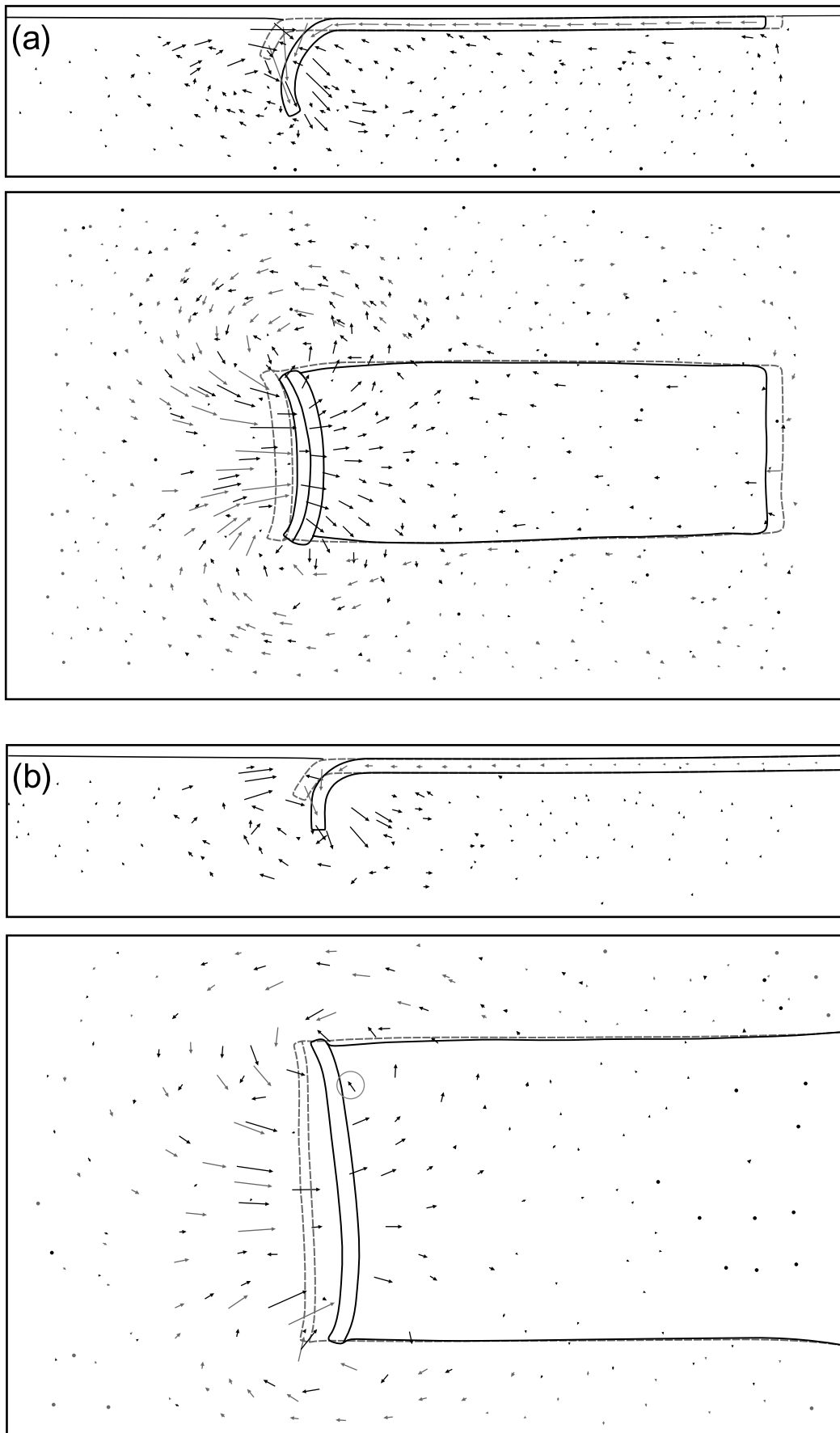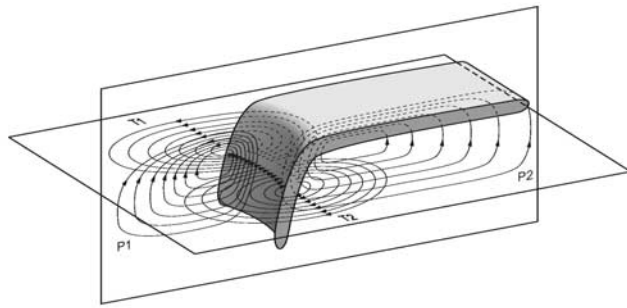
Figure 9

Figure 10. Schematic sketch of subduction and slab rollback-induced flow in the upper mantle. Slab-dip parallel displacement induces two poloidal flow cells with one on each side of the slab. Slab rollback induces two toroidal flow cells with flow around the lateral slab edges.

[29] A schematic diagram illustrating the four dominant flow cells observed in both the fixed and free trailing edge experiments is illustrated in Figure 10. Two poloidal flow cells are plotted, one located in the mantle wedge area and the other underneath the subducting plate, which illustrate the flow induced by displacement of the subducting plate parallel to its own plane. In addition, two toroidal flow cells on either side of the slab edge can be observed, illustrating the slab rollback-induced flow in the mantle. It should be mentioned, though, that these flow cells are a projection of the real flow cells on a horizontal plane. The real flow cells have a tilted rotation axis, which dips in the direction opposite to the direction of slab retreat. Thus mantle material located underneath the slab or in the mantle wedge area above the slab generally has an additional downward component of flow, while mantle material located on the sides of the subducting plate generally has an additional upward component of flow.

[30] A possible explanation for why slab rollback preferentially induces toroidal flow around the slab edges and not flow underneath the slab tip has been illustrated in Figure 11, showing two schematic cross sections through a subduction experiment. The pressure in the glucose syrup in front and behind the slab is in equilibrium, while it is not underneath the slab, as indicated by the elevated isobars, due to sinking of the slab (Figure 11a). Maximum elevation of the isobars is located underneath the lowermost part of the slab tip, due to the maximum amount of slab material above this point. Left of this vertical line, flow is directed toward the left, while right of this vertical line, flow is directed toward the

right (direction of slab retreat). Flow will not be allowed across the line, due to the pressure barrier. Near the lateral slab edges, the flow is directed outward from underneath the slab (Figure 11b).

4. Discussion
4.1. Comparison With Other Dynamic Models
4.1.1. Analogue Models

[31] Results of analogue experiments investigating subduction and rollback have been presented before [*Jacoby*, 1973, 1976; *Kincaid and Olson*, 1987; *Olson and Kincaid*, 1991; *Shemenda*, 1993; *Guillou-Frottier et al.*, 1995; *Griffiths et al.*, 1995; *Faccenna et al.*, 1996, 1999, 2001b; *Buttles and Olson*, 1998; *Becker et al.*, 1999; *Funiciello et al.*, 2002, 2003]. The results described by *Jacoby* [1973], *Kincaid and Olson* [1987], *Funiciello et al.* [2002, 2003] and *Faccenna et al.* [2001b] lend themselves best for comparison, since the model design in these papers is similar to the one presented in this paper.

[32] The results of the free trailing edge experiments can be compared with the model results from *Jacoby* [1973] and *Kincaid and Olson* [1987] with a similar experimental design. *Jacoby* [1973] reports subduction at a constant angle, displacement of the trailing edge and a stable hinge during subduction. However, as reported by the author, the stable hinge is merely related to the width of the model box, which was only slightly wider than the subducting plate and therefore inhibited lateral flow around the slab edges to accommodate for possible slab rollback. Free trailing edge experiments from *Kincaid and Olson* [1987] were reported to show no sign of slab retreat during free sinking of the slab, but only slab retreat when the slab tip would interact with the upper-lower mantle discontinuity. This is in contrast with the results reported here, with significant slab retreat during free sinking of the slab contemporaneously with trailing edge advance, although slab retreat is suppressed with respect to fixed trailing edge experiments (Figure 5). As suggested before, this might be the result of a smaller mantle drag force in the experiments of *Kincaid and Olson* [1987]. In such a scenario, the subducting slab would have displaced itself more parallel to its own plane resulting in a reduction of slab retreat. The viscosity that was used in the experiments of *Kincaid and Olson* [1987] for the upper mantle was 111 Pa·s, which is slightly lower than in the experiments described in here. If the trailing edge migration was also slower in their experiments, then this would have resulted in a smaller mantle drag force.

Figure 9. Line drawings of side-view and bottom-view perspective of two experiments illustrating subduction-induced flow pattern. (a) Experiment 26 (free trailing edge) illustrating flow pattern in glucose syrup before slab tip hits bottom between t = 13 min and 20 seconds s and t = 17 min and 20 s. (b) Experiment 21 (fixed trailing edge) illustrating flow pattern in glucose syrup well before slab tip hits bottom between t = 9 min and t = 14 min. Vectors indicate amount and direction of displacement of passive markers. Dots indicate no displacement. Black vectors are for passive markers in the glucose syrup while gray vectors are for passive markers floating on top of the glucose syrup (bottom view) or passive markers in the side of the subducting plate (side view). Shaded dashed lines and continuous black lines illustrate subducting plate contours at the beginning and end of the time lapse respectively. Encircled vector in (b) points to small component of (oblique oriented) flow underneath the slab tip. Please note that in the side-view diagrams, vectors have been plotted for particles located immediately underneath and in front of the subducting plate as well as for particles located at both sides of the subducting plate. In general, particles moving toward the right (i.e., direction of rollback) are located underneath or in front of the subducting plate, while particles moving toward the left are located to the sides of the subducting plate.
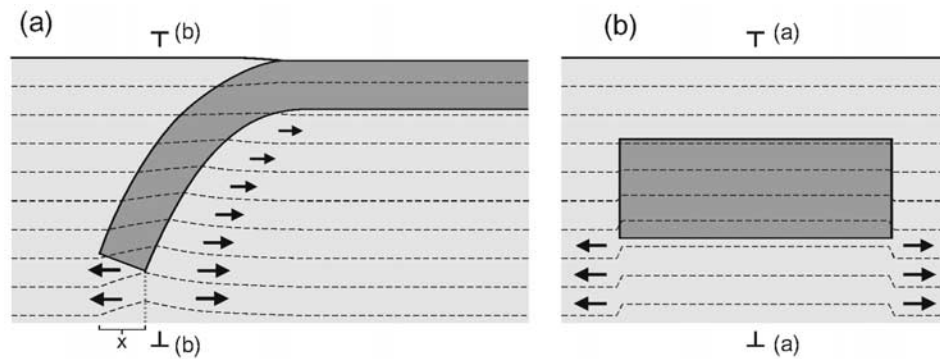
Figure 11. Two schematic cross sections for experiments to illustrate a possible explanation why rollback-induced flow in glucose syrup is oriented only around lateral slab edges and not underneath slab tip. Dashed lines are isobars. Arrows indicate flow direction. (a) Cross section perpendicular to the trench and (b) cross section parallel to the trench. The gray stippled vertical line underneath the slab tip in Figure 11a separates a region of left-directed flow on the left from a region of right-directed flow (e.g., direction of slab rollback) on the right. No flow is allowed across the vertical line because of the pressure barrier. Only material located exactly underneath the slab tip will be forced to flow to the left (region x in Figure 11a). The significance of this flow depends on the kinematics of sinking of the slab. If the slab sinks down vertically it will be larger than when sinking is backward, since in the latter case the material underneath the slab tip will be dragged along with the retreating slab toward the right (e.g., the direction of slab rollback in the diagram of Figure 11a).

However, no data of trailing edge migration versus time are given by *Kincaid and Olson* [1987], which therefore does not allow the drag force to be compared with the experiments described in here.

[33] Comparison of the evolution of the slab geometry between the experiments with a fixed trailing edge reported in here and experiments with a similar experimental design reported elsewhere [*Kincaid and Olson*, 1987; *Faccenna et al.*, 2001b; *Funiciello et al.*, 2002, 2003] shows a good agreement. During free sinking, the slab sinks and rolls back with an increasing slab dip angle until it is subvertical. When the slab tip reaches the upper-lower mantle discontinuity, the slab is draped backward with a horizontal slab segment resting on top of the discontinuity. The slab continues to retreat but with a lower slab dip angle. *Faccenna et al.* [2001b] and *Funiciello et al.* [2002, 2003] also reported an initial exponential increase in hinge retreat during free sinking of the slab, followed by a slowdown during initial contact of the slab with the upper-lower mantle discontinuity, and finally reaching a steady state retreat velocity.

[34] *Buttles and Olson* [1998] and *Funiciello et al.* [2002, 2003] concluded from physical experiments investigating slab rollback-induced mantle flow that poloidal flow underneath the slab tip prevailed in the stage before the slab tip would reach the upper-lower mantle discontinuity. In addition, *Funiciello et al.* [2002, 2003] found that only when the slab tip would interact with the upper-lower mantle discontinuity, the toroidal component of flow around the slab edges would dominate. This is in disagreement with experimental results presented in this paper, where the dominant flow is toroidal-type flow around the lateral edges of the slab. No evidence is found for poloidal flow, where material, initially located under the slab, flows underneath the slab tip toward the mantle wedge.

[35] The discrepancy with the results of *Buttles and Olson* [1998] can be explained by the difference in experimental design and boundary conditions. *Buttles and Olson* [1998] used a slab made of Plexiglas for which slab-dip parallel and slab-dip perpendicular displacement was externally controlled. This could have possibly led to unrealistic flow patterns in the sublithospheric mantle, since the flow did not result from buoyancy-driven subduction forces of the slab such as in nature, but from kinematic boundary conditions externally imposed on the slab.

[36] *Funiciello et al.* [2002, 2003] describe slab-induced flow patterns of experiments with slabs as wide as (laterally constrained) or half the width (laterally unconstrained) of the box. From the former design, it is not surprising that flow would be directed underneath the slab tip, since it is effectively a two-dimensional experiment, comparable to experiments from *Garfunkel et al.* [1986]. *Garfunkel et al.* numerically investigated slab rollback-induced mantle flow in a two-dimensional model box, in which displacement of the slab was externally imposed. Only flow underneath the slab tip was observed due to the two-dimensional setup of the model box. Surprisingly, the streamline pattern illustrating the flow underneath the slab tip in a cross-section view drawn by *Funiciello et al.* [2002, 2003, Figure 4b] is different from the streamline pattern from *Garfunkel et al.* [1986, Figure 7b]. Streamlines drawn by *Garfunkel et al.* [1986] intersect the slab at a steeper angle, pointing to flow underneath the slab tip, while streamlines drawn by *Funiciello et al.* [2002, 2003] intersect the slab at a shallower angle. The discrepancy between the results reported in here and the laterally unconstrained experiments of *Funiciello et al.* [2002, 2003] are unclear, because the experimental design in both cases is very similar and the slab-induced flow was in both cases driven entirely by the negative buoyancy of the subducting lithosphere.

[37] From analogue and numerical experiments, *Becker et al.* [1999], *Faccenna et al.* [2001a, 2001b] and *Funiciello et al.* [2003] found that during free sinking of the slab (e.g.,
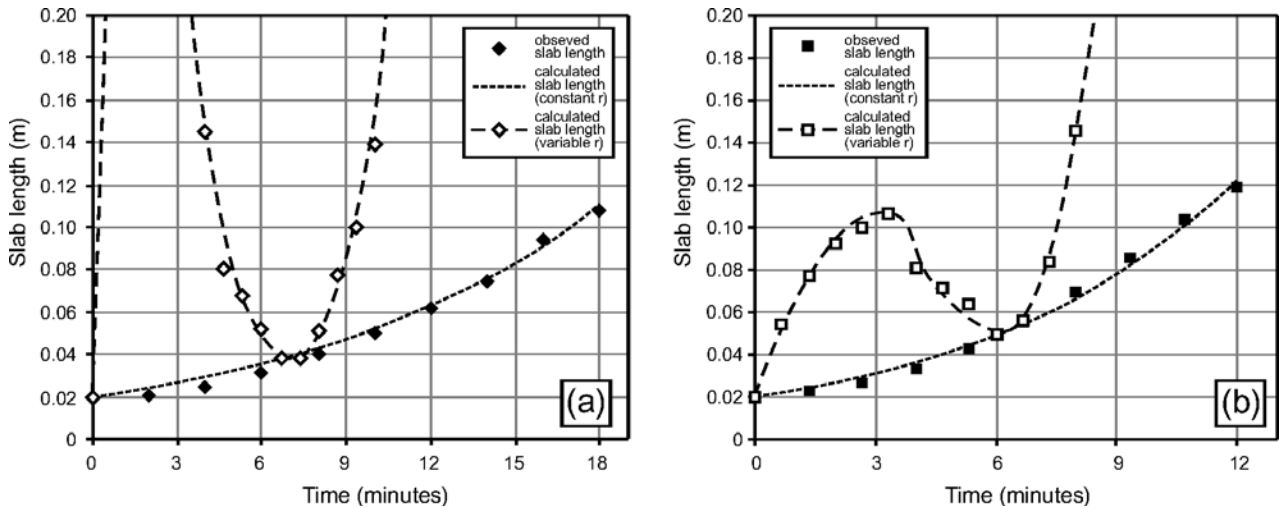
Figure 12. Diagrams illustrating slab length during free fall into upper mantle (free fall stage is defined as the time frame between initiation of subduction and the moment when the slab tip hits the lower discontinuity). Observed slab length is compared with predicted slab length (calculated with equation (3)) for both a constant bending radius (minimum bending radius as observed in experiment (see Figure 13)) and time dependent bending radius as observed in experiment (see Figure 13). (a) Experiment 9 with $C = 0.105$ and minimum bending radius $r = 0.025$ m. (b) Experiment 10 with $C = 0.037$ and minimum bending radius $r = 0.055$ m.

before interaction with the 670 km discontinuity) the slab length $H(t)$ scales as follows:

$$H(t) = H_0 \exp\left(C \frac{\Delta\rho g r^3}{\eta_{sp} R^2} t \right) \qquad (3)$$

where H_0 is the initial slab length, C is a constant, $\Delta\rho$ is the density contrast between slab and mantle, r is the bending radius of the slab, R is the half thickness of the slab, and t is time. Equation (3) has been deduced under the assumption that the bending radius is constant during subduction and that viscous dissipation due to bending of the subducting lithosphere is the main force resisting subduction. The viscous dissipation would therefore be roughly equal to the potential energy dissipation of the subducted slab. Best fit curves for two fixed trailing edge experiments have been plotted in Figure 12 using equation (3). For each experiment two curves have been plotted, one with a time dependent bending radius, as measured from the experiments (Figure 13), and one with a constant bending radius (chosen as the minimum bending radius as observed in the experiment (see Figure 13)). As can be observed in Figure 12, a reasonable fit can be achieved with a constant bending radius and an optimized value for C. For the more realistic case of a time dependent bending radius, however, no satisfying fit can be achieved. This is mainly due to the fact that $H(t)$ in equation (3) is very sensitive to changes in r. The error between calculated and observed slab length curves most likely follows from the initial assumption that the rapidity of subduction during the free fall stage is primarily controlled by the bending resistance. Calculations have shown that the bending resistance accounts for ~30% of resistance to subduction in the initial stage of subduction decreasing to ~15% just before the slab tip hits the lower discontinuity [*Schellart*, 2004]. The better fits between data and curves resulting from equation (3) obtained by *Faccenna*

et al. [2001b] could be explained by the larger viscosity of the slab ($\eta_{sp} = 1.6 \times 10^5$) and viscosity contrast between slab and upper mantle in their experiments ($\eta_{sp}/\eta_m = 350-1000$), compared to the experiments described in here ($\eta_{sp} = 2.4 \times 10^4$, $\eta_{sp}/\eta_m = 185$). These higher values could require a larger component of the driving force to be absorbed by the resistive force to bend the slab, rather than other resistive forces such as shear forces and rollback-induced flow forces. However, it should also be mentioned that the diagrams illustrating subduction in the analogue experiments of *Faccenna et al.* [2001b] (their Figure 3) and *Funiciello et al.* [2003] (their Figures 3 and 8) do show a change in bending radius with progressive time. Therefore
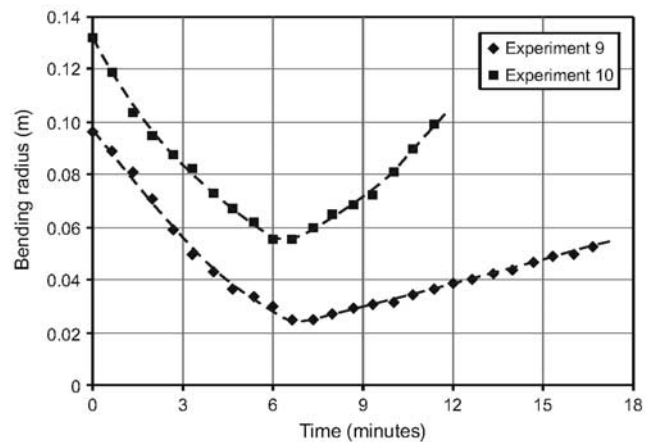

Figure 13. Progressive development of bending radius r during the free fall stage of the slab into the upper mantle for two experiments. Free fall stage is defined as the time frame between initiation of subduction and the moment when the slab tip hits the lower discontinuity.

equation (3) might not be applicable to their experiments as well.

4.1.2. Numerical Models

[38] Numerical experiments on subduction and rollback have been conducted before, but these experiments were in most cases two-dimensional [i.e., *Garfunkel et al.*, 1986; *Giunchi et al.*, 1994; *Marotta and Sabadini*, 1995; *Christensen*, 1996; *Houseman and Gubbins*, 1997; *Olbertz et al.*, 1997; *Becker et al.*, 1999; *Buiter et al.*, 2001; *Cízková et al.*, 2002]. The experimental results presented here have demonstrated that mantle flow around the slab edges is the dominant flow in the upper mantle to allow for slab rollback and no component of rollback-induced flow underneath the slab tip has been observed. The results demonstrate that two-dimensional investigations into slab rollback related processes such as hinge retreat rates [e.g., *Giunchi et al.*, 1994], slab-induced mantle flow patterns [e.g., *Garfunkel et al.*, 1986] and the influence of these flow patterns on slab morphology [e.g., *Marotta and Sabadini*, 1995] could provide unreliable insights. This is because the rollback-induced flow is restricted to a two-dimensional plane oriented perpendicular to the trench and this restriction will therefore significantly and unrealistically influence the experimental outcomes. It could be argued that two-dimensional models of subduction and slab rollback could be representative for natural subduction cases for which the slab is relatively wide. However, even in the case of the South American subduction zone, which is at present the widest and most continuous subduction zone on Earth, shear wave splitting implies that mantle flow in the upper mantle underneath the subducting slab is predominantly oriented parallel to the trench [*Russo and Silver*, 1994, 1996]. Such flow has been suggested to be the result of west-directed retreat of the subducting Nazca plate. Trench-parallel flow underneath the South American slab was already proposed by *Alvarez* [1982], who suggested that the trench-parallel flow would turn eastward near the Caribbean plate and the Scotia plate, forcing the Lesser Antilles arc and Scotia arc to migrate eastward. The South American subduction zone is some 6500 km wide and is much wider than the maximum slab width for experiments described in this paper (with W = 25 cm, corresponding to ~1250 km). Thus the flow pattern in the South American subduction zone might be even more complex than the flow patterns as illustrated in Figures 8 and 9. In any case, trench-parallel flow underneath the South American subduction zone as implied from shear wave splitting points to complex three-dimensional dynamic interaction between the slab and mantle, for which two-dimensional modeling approaches would not suffice.

[39] In a large number of models, a hinge migration velocity was imposed on the subducting lithosphere as a boundary condition, rather then being investigated on its own [e.g., *Garfunkel et al.*, 1986; *Griffiths et al.*, 1995; *Guillou-Frottier et al.*, 1995; *Christensen*, 1996; *Houseman and Gubbins*, 1997; *Olbertz et al.*, 1997; *Buiter et al.*, 2001; *Cízková et al.*, 2002]. From our results it is clear that hinge migration is a transient process, as has been found earlier by *Faccenna et al.* [1996, 1999, 2001b], *Becker et al.* [1999] and *Funiciello et al.* [2002, 2003]. Steady state retreat is only observed when interaction of the slab with the upper-lower mantle discontinuity results in horizontal draping of

the slab over the discontinuity (see also *Funiciello et al.* [2002, 2003]).

4.2. Comparison With Nature

[40] The experimental results of the fixed trailing edge experiments (Figure 2a) lend themselves particularly well for comparison with tomography images across the Calabrian arc [*Lucente et al.*, 1999] and Carpathian arc [*Wortel and Spakman*, 2000], because the horizontal velocity of the subducting and overriding plate in these arc systems is (or was) very low. The Ionian slab subducting along the Calabrian arc is attached to the African plate, which had an absolute velocity of ~3 cm/yr at 30 Ma decreasing to ~1 cm/yr from 10 Ma to Present [*Jolivet and Faccenna*, 2000]. The Carpathian slab was formerly attached to the Eurasian plate, which has been moving at ~1.0–1.5 cm/yr in the last 60 Ma [*Jolivet and Faccenna*, 2000]. In both examples, the slab signature has a relatively steep dip down to the upper-lower mantle discontinuity, where it is deflected horizontally. The deflected part of the slab seems to rest on top of the discontinuity in both cases and continues about as far west as the extent of the backarc basin at the surface (northwest border of Liguro-Provencal Sea for Calabrian arc and southwest border of Pannonian Basin for Carpathian arc). The close resemblance between the slab geometry in nature and experiment would suggest that the slab geometry in both natural cases resulted from eastward slab rollback, which would explain the backarc basins observed at the surface (i.e., Liguro-Provencal Sea and Tyrrhenian Sea for Calabrian arc [e.g., *Malinverno and Ryan*, 1986; *Lonergan and White*, 1997] and Pannonian Basin for Carpathian arc [e.g., *Royden et al.*, 1983]).

[41] Several tomographic images for subduction systems in the Western Pacific show a similar slab geometry including images across the Izu-Bonin arc [*van der Hilst and Seno*, 1993] and across the Kuril arc [*van der Hilst et al.*, 1991]. Again, the slab signature is deflected horizontally at the upper-lower mantle discontinuity. In both cases, the horizontal segment resting on top of the discontinuity underlies a backarc basin at the surface. The Izu-Bonin slab underlies the Parece-Vela backarc Basin which opened from 31 to 15 Ma [*Kobayashi and Nakada*, 1979] and resulted from ~ east directed slab rollback. The Kuril slab underlies the Kuril backarc Basin and the Sea of Okhotsk region, which both formed due to south to southeast directed counterclockwise slab rollback during the Eocene to Miocene [*Schellart et al.*, 2003].

[42] From the experiments it can be concluded that the slab dip is dependent on the retreat velocity, with higher retreat velocities resulting in lower dip angles (Table 2, Figure 7). This supports findings of previous experimental work of subduction and slab rollback [*Griffiths et al.*, 1995; *Guillou-Frottier et al.*, 1995]. The experimental results can be compared to several slabs in nature which are presently retreating (Table 3). The correlation between slab dip angle and hinge retreat velocity is not immediately straightforward, probably because other physical factors influence the slab dip angle as well. For example, the slab dip angle depends on several other factors including absolute velocity of the subducting plate [*Schellart*, 2003], absolute velocity of the overriding plate and buoyancy of the slab [*van Hunen et al.*, 2002]. However, the Tonga-Kermadec subduction

Table 3. Natural Subduction Systems[a]

Subduction System	Retreat, cm/yr	Slab Dip Angle
Hellenic arc	3.0–3.5 (1)	55°
Calabrian arc	6.0 since 5 Ma (2)	70°
Scotia arc	5.7 (3)	70°
Ryukyu arc	4.0 (SW) (4)	40−50°
	1.1 (Central SW) (4)	40−50°
Mariana arc	3.0−4.3 (5)	80−90°
New Hebrides arc	11.8 (SE) (6)	55−60°
	4.2 (Center) (6)	70−75°
Tonga-Kermadec arc	15.9 (NNE) (7)	50°
	9.1 (Central NNE) (7)	55−60°
	1.5−2.0 (SSW) (8)	70−80°

[a]Slab retreat versus slab dip angle. References (in parentheses): 1, *Kahle et al.* [1998] and *McClusky et al.* [2000]; 2, *Faccenna et al.* [2001b]; 3, *Barker* [1995]; 4, *Imanishi et al.* [1996] and *Heki* [1996]; 5, *Martínez et al.* [2000]; 6, *Taylor et al.* [1995]; 7, *Bevis et al.* [1995]; 8, *Wright* [1993].

zone and the New Hebrides subduction zone do show a correlation between the slab dip angle and retreat velocity. For these subduction zones, the absolute velocity of the plate and buoyancy of the slab is approximately constant along the trench. Both subduction zones show an increase in retreat velocity along the trench, which corresponds to a decrease in dip angle of the slab.

[43] All arc-shaped subduction zones, which are or have recently been retreating (as evidenced by the activity in the backarc region) are convex toward the direction of retreat. This has also been observed in the fluid dynamic models. In the models this resulted from toroidal flow in which glucose syrup initially located underneath the slab flowed around the lateral slab edges toward the mantle wedge, forcing the edges of the slab to bend toward the direction of flow. In nature, the convexity of slabs could also be explained in this manner, especially for arc systems, which are presently retreating. Thus lateral slab discontinuities have a major influence on slab retreat and mantle flow patterns and they facilitate rapid slab rollback. However, it should be kept in mind that other factors could also influence the arcuate shape of subduction zones, such as the presence of buoyant irregularities on the subducting plate [e.g., *Vogt*, 1973]. For a number of subduction zones, flow around lateral slab edges toward the mantle wedge region has been implied from volcanic rock geochemistry found in the arc and backarc region. Examples include the Ionian slab subducting underneath the Calabrian arc in the Mediterranean region [*Gvirtzman and Nur*, 1999], the Scotia slab subduction underneath the Scotia arc in the Southern Atlantic [*Livermore et al.*, 1997; *Bruguier and Livermore*, 2001] and the Tonga slab subducting underneath the Tonga arc in the southwest Pacific [*Wendt et al.*, 1997; *Turner and Hawkesworth*, 1998]). In addition, seismic anisotropy for mantle material underneath the Kuril slab near the northern edge of the slab close to the Kuril arc - Aleutian arc intersection implies that mantle material is flowing around the lateral edge of the slab [*Peyton et al.*, 2001].

[44] The most striking evidence for lateral flow around a slab edge is the northernmost Tonga arc region. In the northernmost part of the Tonga region, the NNE-striking subduction zone curves round toward the WNW and changes to a strike-slip zone. At depth, this corresponds to a large vertical edge or tear in the slab. The slab near the tear is itself also curved with a convex shape toward the

east. This is also the direction of slab retreat, as can be implied from the direction of opening of the Lau backarc basin bordering the Tonga arc to the west [*Bevis et al.*, 1995]. Geochemical data for volcanic rocks in the arc and backarc region show signatures of the Samoa mantle plume [*Wendt et al.*, 1997; *Turner and Hawkesworth*, 1998]. This suggest that indeed mantle material located underneath the Tonga slab is flowing toward the north and then turns westward and finally southward around the northernmost edge of the Tonga slab. Thus it can be speculated that eastward retreat of the Tonga slab induces flow around its northern slab edge, which causes the slab and trench to become convex toward the direction of slab retreat.

4.3. Limitations of the Models

[45] As models are simplifications of reality, each model will have its limitations. The models presented in here do not incorporate an overriding plate and therefore the obtained subduction and rollback velocities are likely to be somewhat high, since the subduction fault in the models is very weak and has the same viscosity as the underlying mantle. The subduction fault has a viscosity that is a factor of ∼185 times smaller than the viscosity of the lithosphere. This strength might appear to be very low. However, other modeling investigations have used a very low strength for the subduction fault as well. For example, *Gurnis and Hager* [1988] have modeled subduction with a fault viscosity that is 100 times smaller than the viscosity of the lithosphere.

[46] Also, the models do not incorporate a lower mantle layer and model the upper-lower mantle boundary as a rigid boundary. Thus the models exclude the possibility that subduction and rollback of the slab in the upper mantle will excite flow in the lower mantle. However, penetration of the slab that is restricted to the upper mantle will most likely not be able to excite any flow in the lower mantle, due to the much higher viscosity of the lower mantle compared to the upper mantle. The lower mantle is thought to have a viscosity, which is a factor of 30−100 higher than the viscosity of the upper mantle [*Davies and Richards*, 1992; *Bunge et al.*, 1996; *Conrad and Lithgow-Bertelloni*, 2002]. In addition, it could be argued that a free-slip boundary condition at the core-mantle boundary would facilitate flow in the lower mantle induced by subduction and rollback of a slab located in the upper mantle. However, such a boundary condition would probably not aid very much the overall possibility of lower mantle flow, since this would require the diameter of the flow cell to attain an enormous magnitude. The distance between the upper-lower mantle boundary and the core-mantle boundary is ∼2200 km, and thus, rollback-induced flow along the core-mantle boundary would therefore not be energetically preferable.

5. Conclusions

[47] The experimental results oppose the view that subduction can be regarded as a two-dimensional steady state process. To the contrary, subduction is a three-dimensional process in every aspect of its nature and demonstrates nonsteady state behavior. During subduction and slab rollback, the slab and trench attain an arc-shaped geometry, convex toward the direction of retreat, as also observed for

arc and backarc systems in nature. Subduction and rollback produce a three-dimensional flow pattern with two types of flow cells. Slab-dip parallel displacement produces two poloidal flow cells, one in the mantle wedge above the slab and one underneath the subducting plate. Slab perpendicular displacement (rollback) produces two toroidal-type flow cells, in which material initially located underneath the slab flows around the lateral slab edges toward the mantle wedge. It should be emphasized that the rollback-induced flow is not strictly toroidal, since the rotation axes of the flow cells are not vertical but are tilted and are oriented subparallel to the lateral edges of the slab. No slab rollback-induced flow underneath the tip of the slab is observed except for cases where the slab tip is slanting. In such a scenario, a small amount of toroidal-type flow is observed underneath the shallowest part of the slanting slab tip line. The hinge retreat velocity, dip of the slab and bending radius change in time and in space from initiation of subduction until the slab is draped on top of the upper-lower mantle discontinuity. Only after the frontal segment of the slab has been horizontally draped over the disconti-nuity does the slab approach a steady state with a constant dip angle, constant sinking vectors and a constant retreat velocity. From the experimental results it can be concluded that the following factors enhance slab rollback: (1) an increase in density contrast between slab and sublitho-spheric mantle; (2) a fixed trailing edge boundary condition for the subducting plate rather then a free trailing edge; (3) an increase in slab thickness.

References

Alvarez, W. (1982), Geological evidence for the geographical pattern of mantle return flow and the driving mechanism of plate tectonics, *J. Geophys. Res.*, 87, 6697–6710.

Artyushkov, E. V. (1983), *Geodynamics*, 312 pp., Elsevier Sci., New York.

Barker, P. F. (1995), Tectonic framework of the East Scotia Sea, in *Backarc Basins: Tectonics and Magmatism*, edited by B. Taylor, pp. 281–314, Plenum, New York.

Becker, T. W., C. Faccenna, R. J. O'Connell, and D. Giardini (1999), The development of slabs in the upper mantle: Insights from numerical and laboratory experiments, *J. Geophys. Res.*, 104, 15,207–15,226.

Bevis, M., et al. (1995), Geodetic observations of very rapid convergence and back-arc extension at the Tonga Arc, *Nature*, 374, 249–251.

Bird, P., and K. Piper (1980), Plane-stress finite-element models of tectonic flow in southern California, *Phys. Earth Planet. Inter.*, 21, 158–175.

Bruguier, N. J., and R. A. Livermore (2001), Enhanced magma supply at the southern East Scotia Ridge: Evidence for mantle flow around the subducting slab?, *Earth Planet. Sci. Lett.*, 191, 129–144.

Buiter, S. J. H., R. Govers, and M. J. R. Wortel (2001), A modelling study of vertical surface displacements at convergent plate margins, *Geophys. J. Int.*, 147, 415–427.

Bunge, H.-P., M. A. Richards, and J. R. Baumgardner (1996), Effect of depth-dependent viscosity on the planform of mantle convection, *Nature*, 379, 436–438.

Buttles, J., and P. Olson (1998), A laboratory model of subduction zone anisotropy, *Earth Planet. Sci. Lett.*, 164, 245–262.

Christensen, U. R. (1996), The influence of trench migration on slab pene-tration into the lower mantle, *Earth Planet. Sci. Lett.*, 140, 27–39.

Čízková, H., J. van Hunen, A. P. van den Berg, and N. J. Vlaar (2002), The influence of rheological weakening and yield stress on the interaction of slabs with the 670 km discontinuity, *Earth Planet. Sci. Lett.*, 199, 447–457.

Cloos, M. (1993), Lithospheric buoyancy and collisional orogenesis: Sub-duction of oceanic plateaus, continental margins, island arcs, spreading ridges and seamounts, *Geol. Soc. Am. Bull.*, 105, 715–737.

Conrad, C. P., and B. H. Hager (1999), Effects of plate bending and fault strength at subduction zones on plate dynamics, *J. Geophys. Res.*, 104, 17,551–17,571.

Conrad, C. P., and C. Lithgow-Bertelloni (2002), How mantle slabs drive plate tectonics, *Science*, 298, 207–209.

Conrad, C. P., S. Bilek, and C. Lithgow-Bertelloni (2004), Great earth-quakes and slab pull: Interaction between seismic coupling and plate-slab coupling, *Earth Planet. Sci. Lett.*, 218, 109–122.

Davies, G. F., and M. A. Richards (1992), Mantle convection, *J. Geol.*, 100, 151–206.

Dvorkin, J., A. Nur, G. Mavko, and Z. Ben-Avraham (1993), Narrow sub-ducting slabs and the origin of backarc basins, *Tectonophysics*, 227, 63–79.

Elsasser, W. M. (1971), Sea-floor spreading as thermal convection, *J. Geo-phys. Res.*, 76, 1101–1112.

England, P., and D. McKenzie (1982), A thin viscous sheet model for continental deformation, *Geophys. J. R. Astron. Soc.*, 70, 295–321.

Faccenna, C., P. Davy, J.-P. Brun, R. Funiciello, D. Giardini, M. Mattei, and T. Nalpas (1996), The dynamics of back-arc extension: An experimental approach to the opening of the Tyrrhenian Sea, *Geophys. J. Int.*, 126, 781–795.

Faccenna, C., D. Giardini, P. Davy, and A. Argentieri (1999), Initiation of subduction at Atlantic-type margins; insights from laboratory experi-ments, *J. Geophys. Res.*, 104, 2749–2766.

Faccenna, C., T. W. Becker, F. P. Lucente, L. Jolivet, and F. Rossetti (2001a), History of subduction and back-arc extension in the Central Mediterranean, *Geophys. J. Int.*, 145, 809–820.

Faccenna, C., F. Funiciello, D. Giardini, and P. Lucente (2001b), Episodic back-arc extension during restricted mantle convection in the central Mediterranean, *Earth Planet. Sci. Lett.*, 187, 105–116.

Fukao, Y., S. Widiyantoro, and M. Obayashi (2001), Stagnant slabs in the upper and lower mantle transition region, *Rev. Geophys.*, 39, 291–323.

Funiciello, F., C. Faccenna, D. Giardini, and P. Lucente (2000), Episodic back-arc extension during restricted mantle convection in the Central Mediterranean, *Eos Trans. AGU*, 81(48), Fall Meet. Suppl., Abstract T51E-13.

Funiciello, F., C. Faccenna, D. Giardini, G. Morra, and K. Regenauer-Lieb (2002), Dynamics of retreating slabs: Laboratory and numerical experi-ments, *Boll. Geofis. Teor. Appl.*, 42, supplement 1/2, 170–173.

Funiciello, F., C. Faccenna, D. Giardini, and K. Regenauer-Lieb (2003), Dynamics of retreating slabs: 2. Insights from 3-D laboratory experi-ments, *J. Geophys. Res.*, 108(B4), 2207, doi:10.1029/2001JB000896.

Garfunkel, Z., C. A. Anderson, and G. Schubert (1986), Mantle circulation and the lateral migration of subducted slabs, *J. Geophys. Res.*, 91, 7205–7223.

Giunchi, C., P. Gasperini, R. Sabadini, and G. D'Agostino (1994), The role of subduction on the horizontal motions in the Tyrrhenian Basin: A numerical model, *Geophys. Res. Lett.*, 21, 529–532.

Griffiths, R. W., R. I. Hackney, and R. D. van der Hilst (1995), A laboratory investigation of effects of trench migration on the descent of subducted slabs, *Earth Planet. Sci. Lett.*, 133, 1–17.

Guillou-Frottier, L., J. Buttles, and P. Olson (1995), Laboratory experiments on the structure of subducted lithosphere, *Earth Planet. Sci. Lett.*, 133, 19–34.

Gurnis, M., and B. H. Hager (1988), Controls of the structure of subducted slabs, *Nature*, 335, 317–321.

Gutscher, M.-A., J. Malod, J.-P. Rehault, I. Contrucci, F. Klingelhoefer, L. Mendes-Victor, and W. Spakman (2002), Evidence for active subduc-tion beneath Gibraltar, *Geology*, 30, 1071–1074.

Gvirtzman, Z., and A. Nur (1999), The formation of Mount Etna as the consequence of slab rollback, *Nature*, 401, 782–785.

Heki, K. (1996), Horizontal and vertical crustal movements from three-dimensional very long baseline interferometry kinematic reference frame; implication for the reversal timescale revision, *J. Geophys. Res.*, 101, 3187–3198.

Houseman, G. A., and D. Gubbins (1997), Deformation of subducted oceanic lithosphere, *Geophys. J. Int.*, 131, 535–551.

Imanishi, M., F. Kimata, N. Inamori, R. Miyajima, T. Okuda, K. Takai, K. Hirahara, and T. Kato (1996), Horizontal displacements by GPS measurements at the Okinawa-Sakishima Islands (1994–1995), *Zisin Jishin*, 49, 417–421.

Isacks, B., J. Oliver, and L. R. Sykes (1968), Seismology and the new global tectonics, *J. Geophys. Res.*, 73, 5855–5899.

Jacoby, W. R. (1973), Model Experiment of Plate Movements, *Nature* (Phys. Sci), 242, 130–134.

Jacoby, W. R. (1976), Paraffin model experiment of plate tectonics, *Tecto-nophysics*, 35, 103–113.

Jolivet, L., and C. Faccenna (2000), Mediterranean extension and the Africa-Eurasia collision, *Tectonics*, 19, 1095–1106.

Kahle, H.-G., C. Straub, R. Reilinger, S. McClusky, R. King, K. Hurst, G. Veis, K. Kastens, and P. Cross (1998), The strain rate field in the eastern Mediterranean region, estimated by repeated GPS measurements, *Tectonophysics*, *294*, 237–252.

Kincaid, C., and P. Olson (1987), An experimental study of subduction and slab migration, *J. Geophys. Res.*, *92*, 13,832–13,840.

Kobayashi, K., and M. Nakada (1979), Magnetic anomalies and tectonic evolution of the Shikoku inter-arc basin, in *Geodynamics of the Western Pacific*, edited by S. Uyeda, R. Murphy, and K. Kobayashi, pp. 391–402, Jpn. Sci. Soc. Press, Tokyo.

Le Pichon, X. (1982), Landlocked ocean basins and continental collision: The Eastern Mediterranean as a case example, in *Mountain Building Processes*, edited by K. Hsu, pp. 201–211, Academic, San Diego, Calif.

Livermore, R. A., A. P. Cunningham, L. E. Vanneste, and R. D. Larter (1997), Subduction influence on magma supply at the East Scotia Ridge, *Earth Planet. Sci. Lett.*, *150*, 261–275.

Lonergan, L., and N. White (1997), Origin of the Betic-Rif mountain belt, *Tectonics*, *16*, 504–522.

Lucente, F. P., C. Chiarabba, G. B. Cimini, and D. Giardini (1999), Tomographic constraints on the geodynamic evolution of the Italian region, *J. Geophys. Res.*, *104*, 20,307–20,327.

Malinverno, A., and W. B. F. Ryan (1986), Extension in the Tyrrhenian Sea and shortening in the Apennines as result of arc migration driven by sinking of the lithosphere, *Tectonics*, *5*, 227–245.

Marotta, A. M., and R. Sabadini (1995), The style of the Tyrrhenian subduction, *Geophys. Res. Lett.*, *22*, 747–750.

Martínez, F., P. Fryer, and N. Becker (2000), Geophysical characteristics of the southern Mariana Trough, 11 degrees 50′N–13 degrees 40′N, *J. Geophys. Res.*, *105*, 16,591–16,607.

McClusky, S., et al. (2000), Global positioning system constraints on plate kinematics and dynamics in the eastern Mediterranean and Caucasus, *J. Geophys. Res.*, *105*, 5695–5719.

Molnar, P., and T. Atwater (1978), Interarc spreading and Cordilleran tectonics as alternates related to the age of subducted oceanic lithosphere, *Earth Planet. Sci. Lett.*, *41*, 330–340.

Olbertz, D., M. J. R. Wortel, and U. Hansen (1997), Trench migration and subduction zone geometry, *Geophys. Res. Lett.*, *24*, 221–224.

Olson, P., and C. Kincaid (1991), Experiments on the interaction of thermal convection and compositional layering at the base of the mantle, *J. Geophys. Res.*, *96*, 4347–4354.

Peyton, V., V. Levin, J. Park, M. Brandon, J. Lees, E. Gordeev, and A. Ozerov (2001), Mantle flow at a slab edge; seismic anisotropy in the Kamchatka region, *Geophys. Res. Lett.*, *28*, 379–382.

Ranalli, G. (1995), *Rheology of the Earth*, 413 pp., Chapman and Hall, New York.

Royden, L., F. Horvath, and J. Rumpler (1983), Evolution of the Pannonian Basin system: 1, Tectonics, *Tectonics*, *2*, 63–90.

Russo, R. M., and P. G. Silver (1994), Trench-parallel flow beneath the Nazca Plate from seismic anisotropy, *Science*, *263*, 1105–1111.

Russo, R. M., and P. G. Silver (1996), Cordillera formation, mantle dynamics, and the Wilson cycle, *Geology*, *24*, 511–514.

Schellart, W. P. (2003), Subduction rollback, arc formation and back-arc extension, Ph.D. thesis, Monash Univ., Melbourne, Australia.

Schellart, W. P. (2004), Quantifying the net slab pull force as a driving mechanism for plate tectonics, *Geophys. Res. Lett.*, *31*, L07611, doi:10.1029/2004GL019528.

Schellart, W. P., G. S. Lister, and M. W. Jessell (2002a), Analogue modeling of arc and back-arc deformation in the New Hebrides arc and North Fiji Basin, *Geology*, *30*, 311–314.

Schellart, W. P., G. S. Lister, and M. W. Jessell (2002b), Analogue modelling of asymmetrical back-arc extension, *J. Vir. Expl.*, *7*, 25–42.

Schellart, W. P., G. S. Lister, and M. W. Jessell (2002c), Some experimental insights into arc formation and back-arc extension, *Boll. Geofis. Teor. Appl.*, *42*, supplement 1/2, 85–91.

Schellart, W. P., M. W. Jessell, and G. S. Lister (2003), Asymmetric deformation in the backarc region of the Kuril arc, northwest Pacific: New insights from analogue modeling, *Tectonics*, *22*(5), 1047, doi:10.1029/2002TC001473.

Shemenda, A. I. (1993), Subduction of the lithosphere and back arc dynamics; insights from physical modeling, *J. Geophys. Res.*, *98*(9), 16,167–16,185.

Spakman, W., M. J. R. Wortel, and N. J. Vlaar (1988), The Hellenic subduction zone: A tomographic image and its geodynamic implications, *Geophys. Res. Lett.*, *15*, 60–63.

Taylor, F. W., M. G. Bevis, B. E. Schutz, D. Kuang, J. Recy, S. Calmant, D. Charley, M. Regnier, B. Perin, M. Jackson, and C. Reichenfeld (1995), Geodetic measurements of convergence at the New Hebrides island arc indicate arc fragmentation caused by an impinging aseismic ridge, *Geology*, *23*, 1011–1014.

Turner, S., and C. Hawkesworth (1998), Using geochemistry to map mantle flow beneath the Lau Basin, *Geology*, *26*, 1019–1022.

Uyeda, S., and H. Kanamori (1979), Back-arc opening and the mode of subduction, *J. Geophys. Res.*, *84*, 1049–1061.

van der Hilst, R., and T. Seno (1993), Effects of relative plate motion on the deep structure and penetration depth of slabs below the Izu-Bonin and Mariana island arcs, *Earth Planet. Sci. Lett.*, *120*, 395–407.

van der Hilst, R. D., R. Engdahl, W. Spakman, and G. Nolet (1991), Tomographic imaging of subducted lithosphere below Northwest Pacific island arcs, *Nature*, *353*, 37–43.

van Hunen, J., A. P. van den Berg, and N. J. Vlaar (2002), On the role of subducting oceanic plateaus in the development of shallow flat subduction, *Tectonophysics*, *352*, 317–333.

Vilotte, J. P., M. Daignieres, and R. Madariaga (1982), Numerical modelling of intraplate deformation: Simple mechanical models of continental collision, *J. Geophys. Res.*, *87*, 10,709–10,728.

Vogt, P. R. (1973), Subduction and aseismic ridges, *Nature*, *241*, 189–191.

Wendt, J. I., M. Regelous, K. D. Collerson, and A. Ewart (1997), Evidence for a contribution from two mantle plumes to island-arc lavas from northern Tonga, *Geology*, *25*, 611–614.

Widiyantoro, S., B. L. N. Kennett, and R. D. van der Hilst (1999), Seismic tomography with P and S data reveals lateral variations in the rigidity of deep slabs, *Earth Planet. Sci. Lett.*, *173*, 91–100.

Wortel, R. (1982), Seismicity and rheology of subducted slabs, *Nature*, *296*, 553–556.

Wortel, M. J. R., and W. Spakman (2000), Subduction and slab detachment in the Mediterranean-Carpathian region, *Science*, *290*, 1910–1917.

Wright, I. C. (1993), Pre-spread rifting and heterogeneous volcanism in the southern Havre Trough back-arc basin, *Mar. Geol.*, *113*, 179–200.

_____

W. P. Schellart, Research School of Earth Sciences, Australian National University, Mills Road, Canberra, ACT 0200, Australia. (wouter.schellart@anu.edu.au)